Ocean Dynamics (2018) 68:1457–1479
https://doi.org/10.1007/s10236-018-1204-2

Effect of channel deepening on tidal flow and sediment transport: part I—sandy channels

Leo van Rijn[1] · Bart Grasmeijer[2] · Luitze Perk[3]

Received: 18 February 2017 / Accepted: 12 July 2018 / Published online: 15 August 2018

Abstract
Natural tidal channels often need deepening for navigation purposes (to facilitate larger vessels). Deepening often leads to tidal amplification, salinity intrusion, and increasing sand and mud import. These effects can be modelled and studied by using detailed 3D models. Reliable simplified models for a first quick evaluation are however lacking. This paper presents a simplified model for sand transport in prismatic and converging tidal channels. The simplified model is a local model neglecting horizontal sand transport gradients. The latter can be included by coupling (as post-processing) the simplified model to a 2DH or 3D flow model. Basic sand transport processes in stratified tidal flow are studied based on the typical example of the tidal Rotterdam Waterway in The Netherlands. The objective is to gain quantitative understanding of the effects of channel deepening on tidal penetration, salinity intrusion, tidal asymmetry, residual density-driven flow, and the net tide-integrated sand transport. We firstly study the most relevant tidal parameters at the mouth and along the channel with simple linear tidal models and numerical 2DH and 3D tidal models. We then present a simplified model describing the transport of sand (TSAND) in tidal channels. The TSAND model can be used to compute the variation of the depth-integrated suspended sand transport and total sand transport (incl. bed-load transport) over the tidal cycle. The model can either be used in stand-alone mode or with computed near-bed velocities from a 3D hydrodynamic model as input data.

Keywords Tidal sand transport · Tidal sediment concentrations · Tidal sediment import · Effect of channel deepening

1 Introduction

Most alluvial estuaries have a converging (funnel shaped) planform with a decreasing width in the upstream (landward) direction. The bottom of the tide-dominated section is often fairly horizontal in the entrance region due to dredging for navigation. The passage of large vessels requires water depths of about 10 to 20 m. Some tidal channels have an almost prismatic planform due to the presence of dikes and/or groins. Generally, these structures keep the channel velocities relatively high to prevent deposition.

Tidal systems are affected by various processes: inertia, amplification (funnelling), friction-related damping, reflections, and varying river discharges (Van Rijn 2011a, p. 8.19, 2011b). If the freshwater river discharge is sufficiently large and mixing rates are relatively low, the tidal system is stratified with density-driven residual flow near the bed in landward direction. The combined tide-driven and density-driven velocities are often sufficient to mobilize sand and mud from the bed, the side slopes, and the banks to be transported up and down the tidal channel. The transport of fine sand particles generally is in dynamic equilibrium with the prevailing flow velocity as the upward transport by turbulence and the downward transport by settling proceeds relatively fast (within 15 min) to create saturated transport conditions (as described by sand transport formulae).

An example of a prismatic tidal channel with large water depths is the tidal Rotterdam Waterway in The Netherlands, which is the artificial mouth of the river Rhine and has a length of about 30 km, see Fig. 1. This tidal channel is briefly

Responsible Editor: Bram C. van Prooijen

✉ Leo van Rijn
info@leovanrijn-sediment.com

Bart Grasmeijer
bart.grasmeijer@deltares.nl

Luitze Perk
luitze.perk@waterproofbv.nl

[1] LeoVanRijn-Sediment Consultancy, Blokzijl, The Netherlands

[2] Deltares, Delft, The Netherlands

[3] WaterProof, Lelystad, The Netherlands

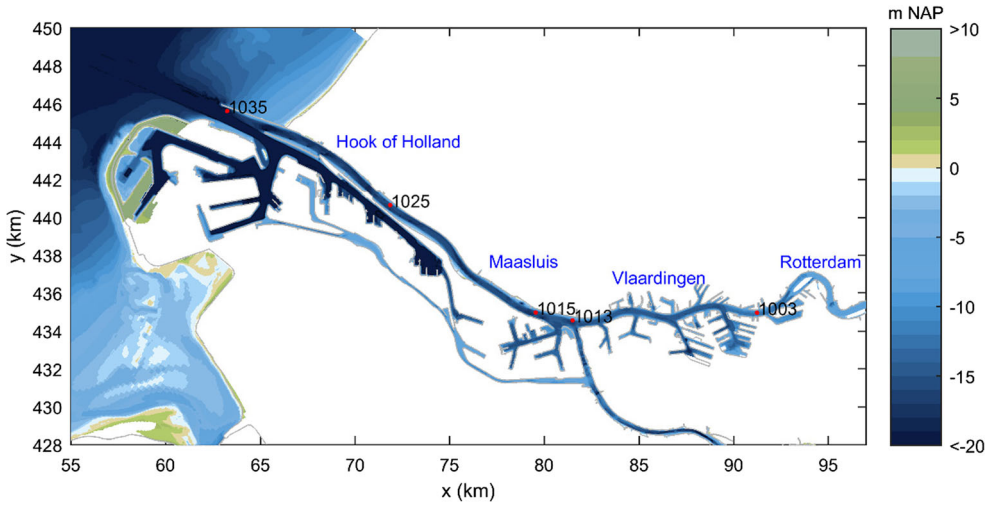

Fig. 1 Plan view and bathymetry (December 2014) of Rotterdam Waterway, The Netherlands (NAP ≅ mean sea level) (Arcadis 2015)

described here, as field data from this case has been used for verification of the various models applied in this part I. More information related to mud is given in part II. The water depth (below mean sea level) of the Waterway decreases stepwise from about 18 m at the mouth to about 11 m near the city of Rotterdam at about 30 km from the mouth and to 8 m more upstream. The tidal range at the mouth is about 1.85 m during mean tidal conditions at present (2017). The annual mean freshwater discharge through the Waterway is about $Q_{\text{waterway},50\%} = 1310$ m^3/s (upstream river discharge at German border of $Q_{\text{upstream},50\%} = 2200$ m^3/s). The bed of the Waterway channel sections is relatively flat (regular dredging) and consists of fine to medium sand (0.2–0.4 mm) with a gradually increasing percentage of mud from 5% at the mouth to 35% at about 20 km from the mouth. During the past decades, the Rotterdam Waterway has undergone a process of constant deepening to accommodate larger vessels calling at the ports of Rotterdam. Plans have been made by the Port Authorities for further deepening (from 15 to 16.3 m between 1010 and 1030 km; see Fig. 1) of some sections of the main navigation channel.

Engineering studies have been done to explore the consequences of the channel deepening of the Rotterdam Waterway (Arcadis 2015). More general research questions related to channel deepening are addressed in these papers (parts I and II): what is the effect of channel deepening on the tide, salinity, and sediment transport characteristics in prismatic and converging tidal channels? Is there a risk of regime change from import to export of sediment (or vice versa), under what conditions, and what are the net annual transport rates involved? Most attention is focussed on prismatic channels based on the example of the Rotterdam Waterway, but converging channels are also addressed.

Various papers of the effects of channel deepening on hydrodynamics and sediment dynamics are available in the international literature; see overview of Van Maren et al. (2015a). Amin (1983) has pointed to changes in tidal constituents due to local channel modifications, channel deepening, and altered hydraulic roughness. DiLorenzo et al. (1993) have found that the mean tidal range near the head of the Delaware Estuary has increased substantially (twofold) due to dredging activities in the middle/upper estuary over the past century. They stated: "The tidal phase-lag between the head of the tide and the entrance decreased from about 9 hours to 6.4 hours. An additional increase of 1.5 m of the navigational channel depth (below Philadelphia) is found (based on numerical simulations) to have a comparatively small or negligible impact on the tidal regime."

Familkhalili and Talke (2016) have used an idealized numerical model to study the effects of channel depth changes on tides and storm surges in the Cape Fear River Estuary. Their model results show that the tidal range in Wilmington is doubled over the last 130 years due to the increase of the local channel depth from 7 to 15.5 m.

Channel deepening not only leads to an increase of tidal penetration, larger tidal ranges (amplification), and peak tidal velocities but may also lead to an increase of tidal velocity asymmetry, salt intrusion, density-driven residual flow near the bed in landward direction, and larger suspended sediment concentrations, transport, and deposition rates, as discussed for the Ems river by Talke et al. (2009), Chernetsky et al. (2010), Winterwerp (2011), Winterwerp and Wang (2013), De Jonge et al. (2014), and Van Maren et al. (2015a). A pronounced tidal asymmetry and density-driven near-bed flow in landward direction were observed in the Ems river (Herrling and Niemeyer 2008; Chernetsky et al. 2010; Talke et al. 2009). The increasing flood-dominated asymmetry strengthens various sediment importing mechanisms in the Ems river related to resuspension, vertical mixing and flocculation (Winterwerp 2011), and lag effects (Chernetsky et al. 2010). Recent semi-analytical model studies show an up-estuary shift of the estuarine turbidity maximum (ETM) due

to channel deepening, changes in tidal asymmetry (Chernetsky et al. 2010), and bed roughness (de Jonge et al. 2014) for the Ems river. Most of these papers are focussed on muddy tidal channels; less attention has been paid to sandy tidal channels, which is the focus of the present paper. Furthermore, most of these papers are site-specific, whereas the present paper has a more general focus using schematic cases of prismatic and converging channels.

This paper studies the effect of channel deepening on the tidal hydrodynamics (Section 3) and sand transport processes (particles > 63 μm) in tidal channels using both simplified and detailed modelling approaches (Sections 2, 3, and 4). This is a follow-up of the papers by Van Rijn (2011b) and Kuijper and Van Rijn (2011).

The simplified sand transport model (TSAND) has been applied with input from a hydrodynamic 2DH or 3D model for the prismatic Rotterdam Waterway case, but the model has also been used in stand-alone mode. Available data on annual sand dredging volumes (Arcadis 2015) of the prismatic Rotterdam Waterway has been used for overall verification of the computed results (Section 4.1).

The proposed simplified model for sand transport in tidal flow (stand-alone mode or coupled to hydrodynamic models) is a new development and can be used for quick evaluation of the most relevant parameters affecting channel deepening. Based on this, the parameter range can be narrowed down substantially to reduce the number of detailed numerical model runs. The stand-alone model has been used to produce a general graph of net tide-integrated sand transport rates as function of water depth and river discharge for sand of 0.25 mm (Section 4.2). This general plot clearly shows the effect of channel deepening on the import or export of sand at the mouth of a tidal channel with a tidal range of about 2 m. This provides both qualitative and quantitative insights of channel deepening effects on sand transport processes. The plot can be used to make a first assessment of the effects of channel deepening on the tide-integrated sand transport rates and hence on dredging volumes. In part II, a similar approach for mud transport (particles < 63 μm) is presented.

Typical examples of muddy rivers with turbidity maxima (increased mud concentrations) in Europe are discussed in part II: tidal Elbe river in Germany, tidal Ems river in Germany, Loire river in France, and Western Scheldt tidal estuary and Rotterdam Waterway (Rhine mouth) in The Netherlands. A simplified mud transport model (TMUD) is described and applied in part II.

2 Model description

2.1 Detailed models

Various detailed hydrodynamic and sediment transport models have been used by the authors. Herein, the leading detailed model is the non-linear Delft3D model for shallow waters, which has been applied in 3D and in 2DH mode. The 3D flow module solves the unsteady shallow water equations in one (1DH), two (2DV or 2DH), or three dimensions (3D). The system of equations consists of the horizontal momentum equations, the continuity equation, the salinity transport equations, and various turbulence closure models. The vertical momentum equation is reduced to the hydrostatic pressure relation as vertical accelerations are assumed to be small compared to the gravitational acceleration and are not taken into account. This makes the 3D model suitable for predicting the flow in shallow seas, coastal areas, estuaries, lagoons, rivers, and lakes. The user may choose whether to solve the hydrodynamic equations on a Cartesian rectangular, orthogonal curvilinear (boundary fitted), spherical grid, or flexible mesh grid. In three-dimensional simulations, a boundary fitted (σ-coordinate) approach as well as a fixed grid are available for the vertical grid direction. The 3D model has been used in combination with submodels for salinity and sediment transport. Various simple sediment transport formulae and the detailed transport model for sand and mud (Van Rijn 1984a, b, c, 2007) have been implemented. The non-linear 2DH and 3D models of the Delft model system have been used and verified extensively in numerous studies (Lesser et al. 2004; Van Rijn 2007, 2011a, b; Van Maren et al. 2015a, b).

The 3D hydrodynamic model of the Port Authority of Rotterdam has also been used. This hydrodynamic model is based on the same equations as the Delft3D model but uses a different schematization with a much finer horizontal grid to better include all geometric details of the Port of Rotterdam with all its docks at the expense of very large run times. This latter model was carefully calibrated to represent the observed water levels (errors within 0.1 m) and the observed salinity distribution (errors within 10% for salt intrusion length) along the Rotterdam Waterway (Arcadis 2015).

2.2 Simplified models

Simple approximations for tidal penetration, peak tidal velocities, tidal asymmetry, salinity-intrusion, density-driven circulation velocities, and tidal sand transport in prismatic and converging models are used (Van Rijn 2011b). In the case of converging channels, the width is represented by $b = b_o \exp(-x/\lambda)$, with the following: b = channel width, b_o = channel width at mouth, λ = converging length scale. A tidal channel is almost prismatic for $\lambda > 300$ km (width reduction of about 65% over 300 km). Strongly converging channels have $\lambda <$ 30 km (width reduction of 65% over 30 km). Weakly converging channels for λ are between 30 and 300 km.

2.2.1 Linear tidal model

The simplest way to study the effect of water depth and channel deepening on the tidal parameters along prismatic and

converging tidal channels is by using a linear tidal model. The classical solution of the linearized mass and momentum balance equations for a prismatic channel of constant depth and width is well known (Lorentz 1922, 1926; Dronkers 1964; Van Rijn 2011a, b). This solution for a prismatic channel represents an exponentially damped sinusoidal wave which dies out gradually in a channel with an open end or is reflected in a channel with a closed landward end. In a frictionless system with depth h_o, both the incoming and reflected wave have a phase speed of $c_o = (gh_o)^{0.5}$ and have equal amplitudes resulting in a standing wave with a virtual wave speed equal to infinity due to superposition of the incoming and reflected wave. Including (linear) friction, the wave speed of each wave is smaller than the classical value c_o (damped co-oscillation). The linear approach can also be used for exponentially converging channels, which has been explained and verified in detail in earlier work (Van Rijn 2011a, b).

It is noted that the linearized solution cannot deal with the various sources of non-linearity such as quadratic friction, large ratio of tidal amplitude and water depth, convective acceleration, variation of the water depth under the crest and trough, effects of river discharges, and effects of tidal flats causing differences in wave speed and hence wave deformation. Therefore, the non-linear Delft3D model (in 2DH mode) has also been used for some cases.

Neglecting the convective acceleration term ($\overline{\overline{u}}\,\partial\overline{\overline{u}}/\partial x$; very small in tidal channels; see Van Rijn 2011a, b), the equations of continuity and motion for depth-averaged flow in a prismatic channel with a rectangular cross section are as follows:

$$\frac{b}{}\frac{\partial\eta}{\partial t} + \frac{\partial Q}{\partial x} = 0 \tag{1}$$

$$\frac{1}{A}\frac{\partial Q}{\partial t} + \frac{g}{}\frac{\partial\eta}{\partial x} + \frac{Q|Q|}{C^2A^2R} = 0 \tag{2}$$

in which $A = b\ h_o$ = area of cross section, b = surface width, h_o = depth to MSL (mean sea level), R = hydraulic radius ($\cong h_o$ if $b >> h_o$), η = water level to mean sea level, Q = discharge = $A\ \overline{\overline{u}}$, $\overline{\overline{u}}$ = cross section-averaged velocity of the main channel, see Fig. 2, A = area of cross section of main channel and C = Chézy coefficient = 5.75 $g^{0.5}\log(12R/k_s)$, and k_s = bed roughness height of Nikuradse (1933).

The equations of continuity and momentum for a wide, prismatic channel with rectangular cross section and constant mean depth ($h = h_o + \eta$) can be linearized (Lorentz method) by replacing the quadratic friction term by a linear term, as follows:

$$\frac{\partial\eta}{\partial t} + \frac{h_o}{}\frac{\partial\overline{\overline{u}}}{\partial x} = 0 \tag{3}$$

$$\frac{\partial\overline{\overline{u}}}{\partial t} + \frac{g}{}\frac{\partial\eta}{\partial x} + m\left|\hat{\overline{u}}\right| = 0 \tag{4}$$

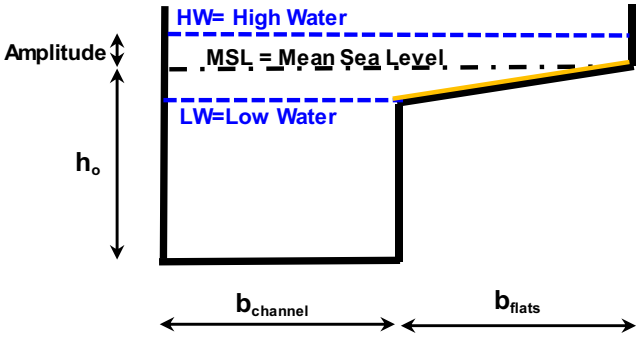

Fig. 2 Schematized cross section of compound channel with main channel and tidal flats

in which $\overline{\overline{u}}$ = cross section-averaged velocity, $\hat{\overline{u}}$ = amplitude of the tidal current velocity, m = linear friction coefficient = $(8g|\hat{\overline{u}}|)/(3\pi C^2 R)$, and R = hydraulic radius ($R \cong h_o$ for a very wide channel $b >> h_o$). Very similar equations can be specified for a compound channel (Fig. 2) with tidal flats (rectangular cross sections of flats and main channel; Van Rijn 2011a).

In the case of a compound cross section consisting of a main channel and tidal flats, it may be assumed that the flow over the tidal flats is of minor importance and only contributes to the tidal storage. The discharge is conveyed through the main channel. This can to some extent be represented by using the following: $c_o = (g\ h_{eff})^{0.5}$ with $h_{eff} = A_c/b_s = \alpha_h\ h_c$ with $\alpha_h = b_c/b_s$: A_c = area of main channel ($= b_c h_c$), h_c = depth of main channel (reduces to h_o without flats), b_c = width of main channel, b_f = width of flats, and $b_s = b_c + b_f$ = surface width.

The transfer of momentum from the main flow to the flow over the tidal flats can be seen as additional drag exerted on the main flow (by shear stresses in the side planes between the main channel and the tidal flats). This effect can be included to some extent by increasing the friction in the main channel slightly. If the hydraulic radius (R) is used to compute the friction parameters (m and C) and the wave propagation depth ($h_{eff} = R$), the tidal wave propagation in a compound channel will be similar to that in a rectangular channel with the same cross section A.

The solution for a prismatic channel is an exponentially damped wave due to bottom friction, as follows:

$$\eta_{x,t} = \hat{\eta}_o[e^{-\mu x}][\cos(\omega t - kx)] \tag{5a}$$

$$\overline{\overline{u}}_{x,t} = \hat{\overline{u}}_o[e^{-\mu x}]\cos(\omega t - kx + \varphi) \tag{5b}$$

$$\hat{\overline{u}}_{x,t} = -\left(\hat{\eta}_o/h_o\right)(\omega/k)[\cos\varphi] = -\left(\hat{\eta}_o/h_o\right)c[\cos\varphi] \tag{5c}$$

with μ = friction parameter, k = wave number, c = wave speed, φ = phase lead of velocity, $H = 2\ \hat{\eta}_o$ = tidal range, $\tan\varphi = \mu/k$, x = horizontal coordinate; positive in landward direction, $\hat{\overline{u}}_o$ = peak tidal velocity of linear model. The detailed solutions for prismatic and converging channels are similar (Van Rijn 2011a, b). It is noted that the linear model is not very accurate for very small water depths (ratio $\hat{\eta}_o\ /h_o$ should be << 1).

2.2.2 Simplified tidal sand transport model (TSAND model)

Definitions We have developed a simplified sand transport model for tidal flow to describe the transport of sand (TSAND). The simplified approach is based on the detailed sediment transport formulations by Van Rijn (2007), which have been verified extensively. The detailed sediment transport formulations have been implemented in the Delft3D model.

The TSAND model can be used in stand-alone mode or in post-processing mode (coupled to hydrodynamic model) to compute the variation of the depth-integrated suspended sand transport and total transport (incl. bed-load transport) over the tidal cycle. It is assumed that the fine sand concentrations are quickly adjusting to local flow conditions (no significant under or overloading). The velocities and sand concentrations are computed as a function of z and t: z = height above bed and t = time (time step of 5 min). The grid points over the depth (50 points) are distributed exponentially as follows: $z = a[h/a]^{(k-1)/(N-1)}$ with the following: a = reference height above bed (input value), $h = h_o + \eta$ = water depth, h_o = depth between bed and mean sea level, η = tidal water level, k = index number of point k, and N = total number of grid points. Used as a stand-alone model, the basic hydrodynamic parameters should be specified by the user. Used as a post-processing model, the hydrodynamic input may come from a 1D, 2DH, or 3D model. TSAND can be used for prismatic and converging channels.

Tidal water levels, flow, and asymmetry The tidal water level at each time t is represented, as follows:

$$\eta_{\mathrm{flood},t} = \eta_{\mathrm{flood,max}} \sin\{\pi(t-\Delta T)/T_{\mathrm{flood}})\} \quad \text{for } t < T_{\mathrm{flood}}$$
$$\eta_{\mathrm{flood,max}} = \gamma_a (H/2) \text{ and } T_{\mathrm{flood}} = \left(\eta_{\mathrm{ebb,max}}/H\right)T \tag{6a}$$

$$\eta_{\mathrm{ebb},t} = \eta_{\mathrm{ebb,max}} \sin\{\pi(t-T_{\mathrm{flood}}-\Delta T)/T_{\mathrm{ebb}})\} \quad \text{for } t > T_{\mathrm{flood}}$$
$$\eta_{\mathrm{ebb,max}} = H-\eta_{\mathrm{flood,max}} \text{ and } T_{\mathrm{ebb}} = \left(\eta_{\mathrm{flood,max}}/H\right)T \tag{6b}$$

with $H = \eta_{\mathrm{flood,max}} + \eta_{\mathrm{ebb,max}}$ = tidal range between the levels of HW and LW, γ_a = asymmetry factor (input value $\gamma_a = 1$ to 1.2, see Fig. 8, $\gamma_a = 1$ yields a symmetrical tide), T = tidal period (input value), ΔT = phase shift (velocity is ahead of water level, input value), T_{flood} = flood period, and T_{ebb} = ebb period. In stand-alone mode, only one representative tide of the neap-spring cycle is considered (H, γ_a, ΔT specified as input by user); the tidal range H comes from the linear tidal model (Section 2.2.1).

The depth-averaged velocity at each time t is represented, as follows:

$$\overline{u}_t = \overline{u}_r + \overline{u}_{\mathrm{max,flood}} \sin(\pi t/T_{\mathrm{flood}}) \quad \text{for } t < T_{\mathrm{flood}}$$
$$\overline{u}_{\mathrm{max,flood}} = \gamma_a\left(\overline{u}_{\mathrm{max}}\right) \tag{7a}$$

$$\overline{u}_t = \overline{u}_r + \overline{u}_{\mathrm{max,ebb}} \sin\{\pi(t-T_{\mathrm{flood}})/T_{\mathrm{ebb}}\} \quad \text{for } t > T_{\mathrm{flood}}$$
$$\overline{u}_{\mathrm{max,ebb}} = -1/\gamma_a\left(\overline{u}_{\mathrm{max}}\right) \tag{7b}$$

with $\overline{u}_t$ = depth-averaged velocity at time t (m/s), $\overline{u}_r$ = net tide-averaged and depth-averaged velocity = $Q/(b\ h)$, b = flow width of channel (input value), h = water depth (input value), and $\overline{u}_{\mathrm{max}}$ = peak tidal velocity of sinusoidal tide (input).

Equations (7a) and (7b) are used to describe the tidal motion of one single tide in the case that the model is used in stand-alone mode. An asymmetrical tide can be generated, using the asymmetry factor γ_a. Tidal flow in various type of channels has been studied to determine the asymmetry factor γ_a (Section 3.3). If the sediment transport model is used as a post-processing model, the near-bed velocity of the hydrodynamic model (1D, 2DH, or 3D) is used as input.

The vertical distribution of the velocity at each time t is represented, as follows:

$$u_{z,t} = u_{\mathrm{rs},z} + \left[\overline{u}_t/(-1+\ln(\mathrm{h}/\mathrm{z_o}))\right]\ln(\mathrm{z}/\mathrm{z_o}) \tag{8}$$

with $u_{\mathrm{rs},z}$ = residual flow velocity due to horizontal salinity-induced density gradient based on Eq. (9), z = level above bed (m), $h = = h_o + \eta_t$ = water depth at time t (m), h_o = tide-averaged water depth (m), η_t = tidal water level (m), $\overline{u}_t$ = depth-averaged flow velocity at time t due to tide + steady river current (m/s), $\overline{u}_r = Q/(bh)$ = river velocity, $z_o = 0.033k_{s,c}$ = zero-velocity level, and $k_{s,c}$ = current-related bed roughness (wave-current interaction is neglected).

The first part of Eq. (8) represents the residual flow due to the density gradient. The depth integration yields zero flow velocity. The second part represents the tidal velocity profile and the river flow velocity profile due to freshwater discharge. The vertical velocity distribution of tidal and river flow is represented by a logarithmic function.

Due to density-driven gravitational circulation, a tide-averaged residual flow is generated in a prismatic channel with tidal flow from the seaside and fresh river water flow from the landside. The residual flow is landward near the bottom and seaward near the water surface. Residual density-induced flow in a prismatic tidal channel can be determined from the tide-averaged momentum equation. There are two main contributions: the free convection contribution arising from the density difference between salt water and

freshwater and the freshwater discharge contribution. The sips mechanism related to tidal straining (Section 1 of part II, see also Burchard and Baumert 1998) which enhances the landward-directed near-bed flow is neglected.

Based on the tide-averaged equation of momentum (including eddy viscosity concept) and no net flow over the depth, the residual (secondary) velocity profile related to density-driven flow can be derived (Hansen and Rattray 1965; Chatwin 1976; Prandle 1985, 2004, 2009). Herein, a similar approach based on a constant vertical eddy viscosity concept is used, resulting in the following (Van Rijn 2011a):

$$\begin{aligned} u_{rs,z} &= M h_o^2 \left[-(1/6)(z/h_o)^3 + (1/2)(z/h_o)^2 - (1/4)(z/h_o)\right] \\ M &= (g\ h_o/E)(1/\rho_m)(\partial\rho_m/\partial x) \\ &= [g^{0.5}C/\{\gamma(|\bar{u}_{max}| + |\bar{u}_r|)\ h_o\}][(h_o/\rho_{fresh})(\partial\rho_m/\partial x)] \end{aligned} \quad (9)$$

with z = level above bed (m), h_o = tide-averaged water depth (m), $\bar{u}_{max}$ = peak tidal velocity, $\bar{u}_r = Q/(bh)$ = river velocity, $z_o = 0.033 k_{s,c}$ = zero-velocity level, $k_{s,c}$ = current-related bed roughness of Nikuradse, M = salinity factor, $E = \gamma\ u_*\ h_o$ = mixing coefficient in near bed zone (constant), $u_* = (g^{0.5}/C)\ (|U_{max}| + |\bar{u}_r|)$, C = Chézy coefficient = $5.75\ g^{0.5}\log(12h/k_{s,c})$, ρ_{sea} = density of sea water (kg/m^3), $\partial\rho_m/\partial x$ = salinity-induced horizontal density gradient, ρ_m = depth-averaged and tide-averaged fluid density due to salinity = $\rho_{fresh} + 0.77S$ (kg/m^3), ρ_{fresh} = fresh water density, S = salinity value (0 to 30 kg/m^3), and γ = coefficient (0.003 based on calibration; see part II). The maximum residual velocity of Eq. (9) is approximately $u_{s,max} = -0.035 M h_o^2$ at about $z/h_o = 0.3$.

Equation (9) is valid in the mouth region of a tidal channel where the vertical density profile is partially mixed over the depth. The residual velocities are maximum in the near-bed region and show increasing residual velocities for increasing water depth and increasing river discharge. The vertical mixing coefficient E (or γ) is used as calibration parameter, which is discussed in part II based on measured and computed (3D model) data of the Rotterdam Waterway.

Equation (9) is very similar to that of Hansen and Rattray (1965), Chatwin (1976), and Prandle (1985, 2004, 2009). The latter was derived for a partially mixed estuary: $u_{s,max} = M h_o^2$ [− (1/6) $(z/h_o)^3 + 0.27\ (z/h_o)^2 - 0.037\ (z/h_o) - 0.029$], which yields $u_{s,max} \cong -0.03 M h_o^2$ at about $z = 0.1$ h. It is noted that the expression of Prandle yields a finite residual velocity value at $z = 0$ (at the bed), whereas Eq. (9) yields a zero residual velocity at the bed.

The residual velocities generated by density differences due to strong horizontal sediment concentration gradients, which may occur in the high turbidity zone (Talke et al. 2009), have been neglected. Hence, the model is less accurate when it is used in stand-alone mode for the estuarine turbidity maximum (ETM) with relatively high horizontal sediment density variations.

Sediment concentrations and transport The sand concentrations are computed using a multi-fraction method (Van Rijn 2007). The multi-fraction method is based on $N = 6$ fractions (0.062–0.125, 0.125–0.2, 0.2–0.3, 0.3–0.5, 0.5–1, 1–2 mm). The single fraction method is obtained for $N = 1$. The sand concentration profile at each time t is represented by an analytical expression, as follows:

$$c_i = c_{a,i}[((h-z)/z)(a/(h-a))]^{ZSi} \quad (10)$$

with c_i = concentration of fraction i (kg/m^3), ZS_i = suspension number of sediment fraction i (−).

The reference concentration c_a of fraction i at reference level $z = a$ is represented as follows (Van Rijn 2007, part II):

$$c_{a,i} = 0.015\ \ \alpha_{ca}(1-p_{mud})\ \ (d_i/a)\ \ (T_i)^{1.5}\left(D_{*,i}\right)^{-0.3} \quad (11)$$

with α_{ca} = correction/scaling coefficient (default = 1), d_{50} = median particle diameter, a = input value, $D_{*,i} = d_i[(s-1)g/\nu^2]^{0.333}$ = dimensionless particle parameter, $T_i = [\lambda_i(\tau_b' - \chi\ \zeta_i\ \tau_{b,cr,d50})]/[\chi(d_i/d_{50})\tau_{b,cr,d50}]$ = dimensionless bed-shear stress parameter of fraction i, $\tau_{b,cr,d50}$ = critical bed-shear stress of sand based on d_{50}, $\tau_b' = \mu_c\tau_{b,c} + \mu_w\tau_{b,w}$ = effective bed-shear stress due to current and waves, $s = \rho_s/\rho$ = relative density, $\chi = (1 + p_{gravel})(1 + p_{mud})^3$ = factor representing effect of mud and gravel on the critical shear stress of sand, $\lambda_i = (d_i/d_{50})^{0.25}$ = roughness correction factor of fraction i, $\zeta_i = (d_{50}/d_i)^{0.5}$ = hiding-exposure factor of fraction i (maximum 2 and minimum 0.5), ν = kinematic viscosity coefficient, ρ_s = sediment density (input value), ρ = fluid density, p_{mud} = fraction of mud (< 0.063 mm) of top layer of bed (0 to 0.3), and p_{gravel} = fraction of gravel (> 2 mm) of top layer of bed (0 to 0.1).

Equation (11) can be used for both sand (part I), silt, and mud (part II).

The critical bed-shear stress of sand is represented by the following (shields based on d_{50}):

$$\tau_{b,cr,sand} = (\rho_s - \rho)\ g\ d_{50}\ \left[0.3/D_* + 0.055\left(1 - e^{-0.02D_*}\right)\right] \quad (12)$$

The critical bed-shear stress for erosion of mud (part II) is an input parameter to deal with site-specific conditions (no general relationship is available).

The bed-shear stresses at time t due to currents and waves are represented as follows:

$$\tau_{b,c} = \rho\ \left(u_{*,c}\right)^2 \text{ with } u_{*,c} = \kappa\ u_z/\ln\left(30z/k_{s,c}\right) \quad (13)$$

$$\tau_{b,w} = 0.25\ \rho\ f_w\ (U_w)^2 \quad (14)$$

with $\kappa = 0.4$ and u_z = flow velocity at $z \cong 0.1$ h, $U_w = (2\pi/T_p)A_w$ = peak orbital velocity (linear wave theory), A_w = peak orbital excursion, T_p = peak wave period, $f_w = \exp(-6 + 5.2(A_w/k_{s,w}))^{-0.19})$ = wave-related friction coefficient, ρ = fluid density including salinity effect, $k_{s,c}$ = current-related roughness, and $k_{s,w}$

= wave-related roughness. The effect of surface waves is included to deal with waves in the mouth of a tidal channel.

The effective bed-shear stresses at time t for sediment transport are represented as follows:

$$\tau_{b,c}{}' = \mu_c \, \tau_{b,c} \tag{15}$$

$$\tau_{b,w}{}' = \mu_w \, \tau_{b,w} \tag{16}$$

with $\mu_c = f_c'/f_c$ = current-related efficiency factor, $f_c = 0.24/(\log(12\ h/k_{s,c}))^2$ = current-related friction coefficient, $f_c' = 0.24/(\log(12\ h/d_{90}))^2$ = grain-related friction coefficient, d_{90} = grain size, $\mu_w = 0.7/D_*$ = wave-related efficiency factor ($\mu_{w,min} = 0.14$, $\mu_{w,max} = 0.35$).

The suspension number ZS of sand is represented as follows:

$$\begin{aligned} ZS_{sand,i} &= w_{sand,i,o}/\left(\beta\kappa u_{*,cw}\right) \\ &+ 2.5\left(w_{sand,o}/u_{*,cw}\right)^{0.8}\left(c_{a,sand}/c_o\right)^{0.4} \\ &+ \left(\rho/\rho_{fresh}-1\right)^{0.4} \end{aligned} \tag{17}$$

with $w_{sand,i,o}$ = fall velocity of fraction i (based on formula Van Rijn 1993), $\kappa = 0.4$, $\beta = 1 + 2(w_{sand,i}/u_{*,cw})^2$ = coefficient ($\beta_{max} = 1.5$), $u_{*,cw} = (u_{*,c}{}^2 + u_{*,w}{}^2)^{0.5}$ = bed-shear velocity due to current and waves, $u_{*,c} = (\tau_{b,c}/\rho)^{0.5}$ = current-related bed-shear stress, $u_{*,w} = (\tau_{b,w}/\rho)^{0.5}$ = wave-related bed-shear stress, c_a = reference concentration, $c_o = 0.65$ = maximum bed concentration, ρ = fluid density including salinity effects, and ρ_{fresh} = fluid density of freshwater (= 1000 kg/m^3).

Equation (17) represents the effects of downward gravity settling, upward turbulence mixing (first term), empirical damping due to vertical sediment concentration gradients (second term), and empirical damping due to vertical salinity gradients (third term) (Winterwerp 2001; Van Rijn 1993). The damping due to vertical salinity/density gradients mainly occurs during the flood period when the salt wedge penetrates landward. A larger ZS value yields smaller concentrations.

The time lag effect of the suspended concentrations and suspended transport rate can be represented to some extent by applying an exponential adjustment of the reference concentration at time t based on $dc_a/dt = -A(c_{a,t} - c_{a,eq,t})$, resulting in the following (Van Rijn 2015):

$$\begin{aligned} c_{a,t} &= c_{a,t-\Delta t} + dc_a \\ c_{a,t} &= \left[1/(1 + A\ \ \Delta t)\right]\left[c_{a,t-\Delta t} + A\ \ \Delta t\ \ c_{a,eq,t}\right] \end{aligned} \tag{18}$$

with Δt = time step (5 min), $c_{a,t\ -\Delta t}$ = suspended reference concentration at previous time ($\sum c_{a,i}$ for multifraction method), and $c_{a,eq,t}$ = equilibrium reference concentration at time t,

$$A = \gamma_c 0.05(1/h)\left(w_{sand,o}/u_{*,cw}\right)\left(1 + 2w_{sand,o}/u_{*,cw}\right) \left(1 + H_s/h\right)^2, A_{minimum} = 0.0005,$$

γ_c = calibration coefficient (range 0.5 to 2; default = 1).

The suspended transport q_s can be computed by integration of the product of velocity and concentration over the water depth:

$$\begin{aligned} q_s &= {}_o\sum^N {}_a\sum^h (u\ c)\ dz \quad \text{with } N = 6 \\ &= \text{number of fractions} \\ &\quad \text{(summation over fractions and depth)} \end{aligned} \tag{19}$$

The bed load transport (in kg/m/s) is computed by using a simplified expression (Van Rijn 2007).

The total load transport at each time t is computed as follows: $q_{tot} = q_s + q_b$.

The tide-integrated sediment transport rates are computed by integration over the tidal cycle.

Verification of sand transport model The simplified approach presented here is based on the detailed sediment transport formulations by Van Rijn (1984a, b, c, 1993, 2007, 2015), which have been verified extensively for river and tidal flow. The detailed formulations have been implemented in the Delft3D modelling suite and the approach presented here is basically a simplified version of the detailed numerical model.

The detailed sand transport model has been verified many times before (Van Rijn 1984a, b, c, 1987, 2007; Lesser et al. 2004). Herein, only one high-quality data set for tidal flow is considered. This case refers to measured sand concentrations and velocities in a tidal channel of the Eastern Scheldt estuary in the southwest part of The Netherlands (Krammer, Station 2, April 8, 1987; Voogt et al. 1991). The data set based on classical mechanical sampling instruments represents a wide range of velocities (1.4 to 1.9 m/s) and is a high-quality data set. The measured suspended transport has a relative error of about 30% (Voogt et al. 1991).

The water depths are in the range of 7 to 8 m. Water depth variations are due to tidal water level variations and the presence of mega-ripples (with height of about 0.5 m). The bed material is sand with $d_{50} = 0.3$ mm and $d_{90} = 0.6$ mm (six fractions $p_1 = 0.04$, $p_2 = 0.15$, $p_3 = 0.35$, $p_4 = 0.45$, $p_5 = 0.01$, $p_6 = 0$).

Model validation results are given in Fig. 3 presenting the measured water depths, measured depth mean velocities, measured suspended transport rates, and the computed suspended transport rates based on the single fraction and multi fraction methods (TSAND model) without any calibration. The bed roughness is taken to be $k_s = 0.4$ m based on measured velocity data. The depth mean velocity increases from about 1.1 m/s to about 1.9 m/s at peak flow conditions resulting in a strong increase of the suspended transport. The computed suspended transport rates of the multi fraction method are in good agreement with measured values (all results within factor 2), although the computed model results are, on average, somewhat too small. The computed suspended transport rates based on the single fraction method with $d_{sus} = d_{50} = 0.3$ mm are too small (factor 2). The single fraction method produces good

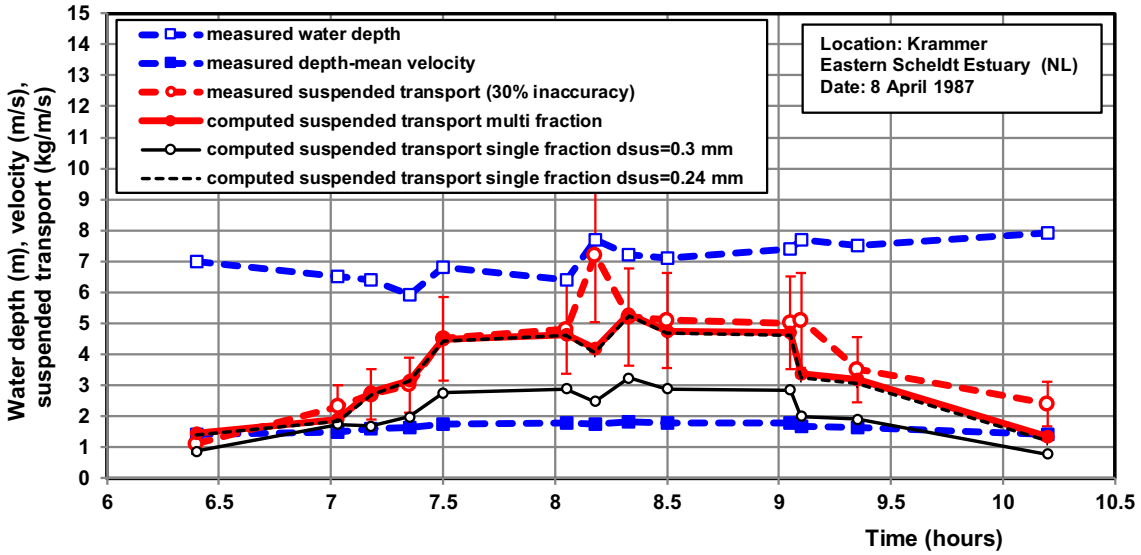

Fig. 3 Measured and computed suspended sand transport in tidal channel Krammer, Eastern Scheldt, The Netherlands (Voogt et al. 1991)

results if the suspended sediment size is calibrated to be $d_{sus} = 0.8d_{50} = 0.24$ mm, which is in agreement with earlier findings (Van Rijn 1984a, b, c).

3 Effect of channel deepening on tidal parameters

To operate the TSAND model in stand-alone mode for schematic and practical cases (Section 4.2), it is essential to have knowledge of the peak tidal velocities in the mouth region (length < 0.1 tidal wave length) and the velocity asymmetries involved. We will therefore now study these parameters and the effects of channel deepening on these parameters by using linear and non-linear models focussing on various schematic cases with varying water depth.

3.1 Tidal range and tidal penetration

In the case of a prismatic channel, the linear model solution is a damped tidal wave with a damping rate depending on the water depth and the bed roughness. In the case of a converging tidal channel, the solution can be a damped tidal wave or an amplified tidal wave depending on the converging length scale, the water depth, and the bed roughness (Friedrichs 2010, Van Rijn 2011a, b). It has been shown that the linear model works very well for a wide range of conditions (Western Scheldt estuary (Netherlands), Hooghly estuary (India), Delaware estuary (USA), and the Yangtze estuary in China (Van Rijn 2011a, b).

We have used the linear model to compute the reduction of the tidal range (H/H_o) in a prismatic channel with water depths in the range of 11 to 17 m and channel width of 500 m, see Fig. 4.

Two cases with different depth conditions are distinguished: Rotterdam Waterway in the year 1910 with a depth in the range of 8 to 12 m and in the year 2017 with a depth range of 8 to 18 m. The tidal range at the mouth is $H_o \cong 1.65$ m in 1910 (Hollebrandse 2005) and 1.85 m in 2017 (Rijkswaterstaat 2017). The tidal period is 44,700 s. The applied bed roughness is set to 0.05 m. Measured tidal range values in 2017 are available for four stations (Figs. 1 and 4) and in 1910 for one station Rotterdam (Rijkwaterstaat 2017; Van de Kreeke and Haring 1979).

The longitudinal bottom profile of the Rotterdam Waterway in 2017 consists of various sections with different water depths (h_i) between 18 and 8 m to MSL (mean sea level) and different lengths (L_i) between 4 and 19 km ($L_t = 45$ km = total length). As tidal penetration is found to be proportional to $h^{1.8}$ (see below), the effective water depth has been determined as $h_e = \sum(h_i^{1.8} L_i/L_t)$, resulting in the weighted value $h_e = 13.5$ m for the present situation in 2017. The effective depth in 1910 is about 10 m. The depth mean river velocity (river discharge divided by cross-sectional area) is about 0.15 m/s, which is small compared to the peak tidal velocity of about 1 m/s. The river velocity effect on the tide cannot be taken into account by the linear model. Using the effective depth values, the linear model yields a tidal range reduction of about 18% over 30 km (Rotterdam) in 1910 and 13% in 2017, which is somewhat higher than the measured values of 14% in 1910 and 11% in 2017 (Fig. 4). This can easily be improved by using a smaller bed roughness value (calibration). Echo sounding results of the bed surface shows a rather flat bed without the presence of bed forms (Arcadis 2015). Hence, a small roughness value in the range of 0.01 to 0.05 m is realistic. The linear model and the measured data show that the damping is less for a larger depth, but the effects are relatively small.

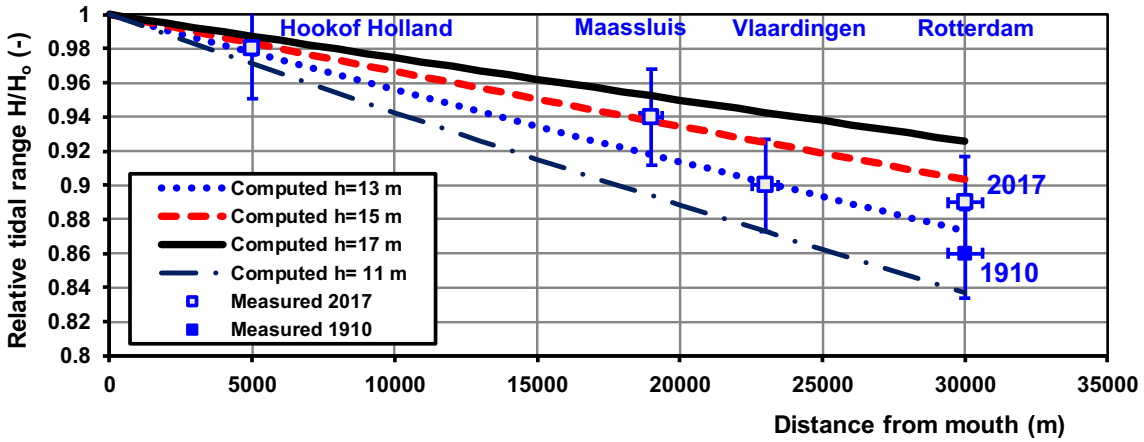

Fig. 4 Effect of water depth on the reduction of tidal range along the prismatic tidal channel of the Rotterdam Waterway in 1910 and 2017 based on linear tidal model ($k_s = 0.05$ m)

Hereafter, the linear model is used to study the tidal penetration distance (L_p) as function of water depth, bed roughness and the presence of tidal flats (compound prismatic channel) for a range of conditions, see Fig. 5. The tidal penetration distance is defined as the distance after which the tidal amplitude is smaller than 1% of that at the mouth. Water depth, bed roughness, and tidal flats are the most influential parameters. It is clear that tidal penetration increases strongly for increasing water depth (less friction), roughly $L_p \sim h_o^{1.8}$ for $k_s = 0.01$ m (see Fig. 5) and $L_p \sim h_o^{1.5}$ for $k_s = 0.1$ m (see Fig. 5) for situations with no tidal flats. Tidal penetration increases for decreasing bed roughness k_s (from 0.1 to 0.01 m). Tidal penetration is strongly affected by the presence of tidal flats. The bed of the tidal flats is assumed to be between LW (low water level) and MSL (mean sea level), see Fig. 2. We have used two values of the width of the tidal flats: $b_{flats} = 0.5\ b_{channel}$ and $b_{flats} = b_{channel}$. The channel width is set to 500 m. As can be seen, the presence of tidal flats yields a significant reduction (more than 50%) of the tidal penetration length. This underlines the importance of the tidal flats (see also Friedrichs and Aubrey 1988). Removal of tidal flats leads to larger tidal penetration and associated salinity intrusion. In practice, the effect of tidal flats is much less as tidal flats are usually only present in the outer part of the estuary. Tidal flats in the middle part of the estuary are often reclaimed for commercial use.

3.2 Peak tidal velocity at mouth

The magnitude and direction of tidal sand transport in the mouth region strongly depends on the peak velocities of the tidal system in that region and are discussed in this section. The horizontal distribution of the peak tidal velocities along the tidal channel beyond the mouth region is discussed in Section 3.4.

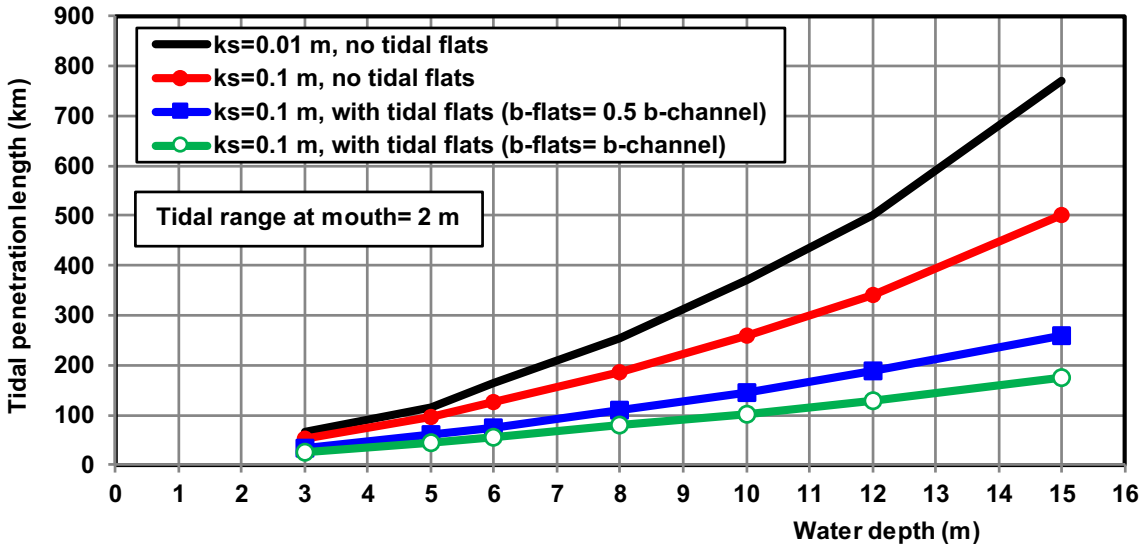

Fig. 5 Effect of water depth, bed roughness, and tidal flats on tidal penetration for a prismatic tidal channel based on linear tidal model

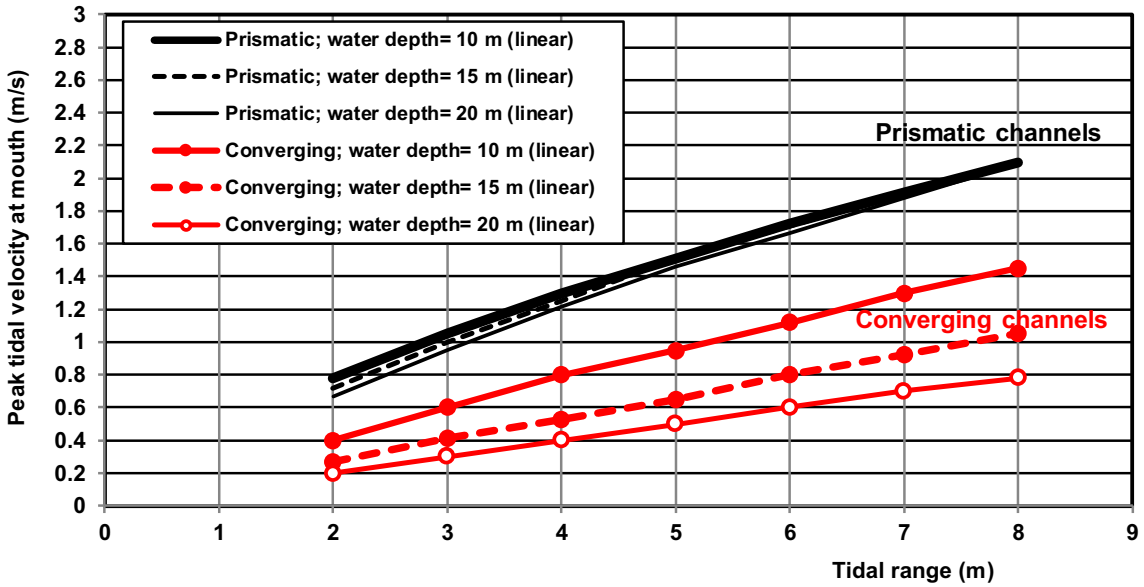

Fig. 6 Effect of water depth and tidal range on the peak tidal velocity at the mouth for prismatic and converging channels based on linear model (bed roughness = 0.05 m)

We have used the linear model and non-linear models to compute the peak tidal velocity at the mouth of various tidal channels and the phase shift between the vertical and horizontal tides. The peak tidal velocity at the mouth based on the linear model primarily depends on the type of channel (prismatic or converging), the tidal range, the water depth, and the bed roughness, see Fig. 6 for the linear model results and Fig. 7 for both linear and non-linear models. The converging case is a strongly converging tidal channel with a length of 60 km (<< tidal wave length) and a mouth width of 25 km reducing (exponentially) to about 2 km at 60 km (resembling the Western Scheldt, The Netherlands).

In the case of prismatic channels, the peak velocity at the mouth increases from about 0.8 m/s at a tidal range of 2 m to about 2 m/s at a tidal range of 8 m based on Eq. (5c). The effect of the water depth (between 10 and 20 m) is marginal for prismatic channels; the peak velocity is slightly smaller for a larger depth. A smaller bed roughness of $k_s = 0.01$ m (factor 5 smaller) leads to somewhat larger velocities (about 5%). A larger bed roughness of $k_s = 0.25$ m (factor 5) leads to somewhat smaller velocities (about 7%). The phase lead between the horizontal and vertical tide in prismatic channels decreases from about 1.2 to 0.7 h for increasing water depths between 5 and 15 m (not shown). The phase lead is almost zero for a

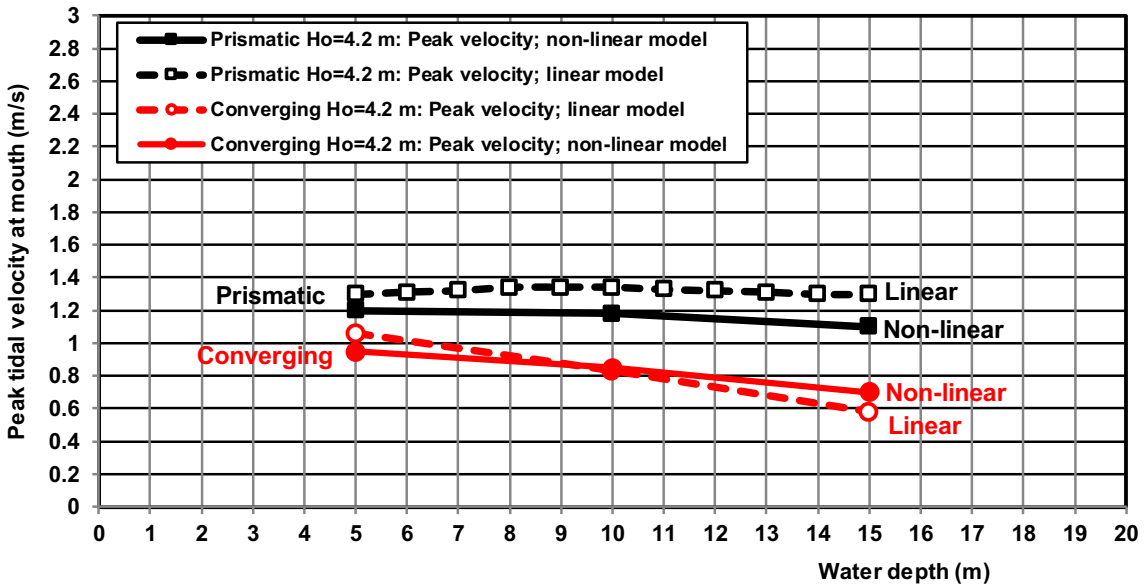

Fig. 7 Effect of water depth on the peak tidal velocity at the mouth for prismatic and converging channels based on linear and non-linear 2DH Delft model (tidal range = 4.2 m; bed roughness = 0.05 m)

depth of 50 m. In a prismatic channel, the phase lead of the linear model only depends on the bottom friction and is fairly accurate.

In the case of a strongly converging channel with a mouth width of 25 km reducing (exponentially) to about 2 km at 60 km from the mouth, the peak velocities at the mouth are much smaller compared to those in prismatic channels. The effect of the water depth is much stronger. Increasing the water depth from 10 to 20 m leads to a velocity decrease of about 40%. In a converging channel, the predicted phase lead of the linear model is less accurate as it depends on bottom friction and on the converging length scale, which introduces additional schematization errors (Van Rijn 2011a, b).

A comparison of linear and non-linear model results is given in Fig. 7, which shows the peak tidal velocity as function of the water depth for a constant tidal range of 4.2 m (about the middle of the tidal range interval of Fig. 6). The peak velocity of the non-linear 2DH model represents the average value of the peak flood and ebb values. The computed results of the linear model and the non-linear 2DH Delft model for a tidal range of 4.2 m are fairly similar. The linear model, although strictly valid for $\hat{\eta}_o \ll h_o$), does surprisingly well for shallow depths ($\hat{\eta}_o / h_o \cong 0.3$–$0.4$).

The relationship between the peak tidal velocity at the mouth and the water depth in prismatic channels can be determined analytically using Eq. (5c) of the linear model. Based on sensitivity computations using the linear model, the wave speed c in water depth between 5 and 20 m is roughly proportional to $c \sim h_o^{0.7}$ and the phase lead ($\cos\varphi$) is proportional to $\cos(\varphi) \sim h_o^{0.1}$. The phase lead is about 1.5 h for a very shallow prismatic channel (relatively large friction) and about zero for a very deep channel (almost no friction). The value of $\cos(\varphi)$ varies very weakly between 0.8 and 1. Given these results, the peak tidal velocity (Eq. 5c) at the mouth of a prismatic channel without flats varies roughly as follows: $\hat{\overline{u}}_o \sim h_o^{-0.2}$ yielding a weakly decreasing curve for increasing channel depths, as shown in Fig. 7.

Thus, channel deepening has a very marginal effect on the peak tidal velocity in a relatively wide prismatic channel. In a strongly converging tidal channel, the peak tidal velocity reduces by about 30% if the water depth increases (factor 3) from 5 to 15 m. Other configurations can be easily explored by the analytical linear model equations.

3.3 Tidal asymmetry at the mouth

The analytical solutions of the linearized equations of continuity and momentum presented above do not express the non-linear effects. All non-linear terms ($\overline{u}\,\partial\overline{u}/\partial x$; $\partial(\eta\overline{u})/\partial x$ and u^2) have been neglected or linearized. Thus, the wave speed is constant and the peak flood and ebb velocities are equal (no asymmetry).

Friedrichs and Aubrey (1988) have shown for a short estuary without upstream river flow that the velocity asymmetry depends on the relative tidal amplitude ($\hat{\eta}_o / h_o$) and the ratio V_s/V_c with $\hat{\eta}_o$ = tidal amplitude, h_o = water depth to mean sea level, V_s = intertidal water volume between HW and LW above the flats, and V_c = water volume in main channel below mean sea level. A ratio $V_s/V_c \cong 0$ means the presence of a channel without tidal flats resulting in flood dominance ($\gamma_a = \hat{\overline{u}}_{flood} / \hat{\overline{u}}_{ebb} > 1$). Ebb dominance can occur if the propagation of the tide during flood is slowed down sufficiently by the water mass above the tidal flats. During ebb, the flats are dry and the tide propagates through the main channel at a smaller water depth with larger flow velocities resulting in ebb dominance. It is shown that ebb-dominant sand transport prevails at the mouth of shallow estuaries for $\hat{\eta}_o / h_o < 0.3$ with $V_s/V_c > 0.3$, which cover many small-scale estuaries in the USA. Flood dominance prevails for all conditions without flats. Thus, flood dominance occurs in shallow, narrow channels, and ebb dominance in deeper channels with flats. Hence, shallow channels tend become shallower due to sediment import (flood dominance) and deeper channels tend to become deeper due to sediment export (ebb dominance) for tidal channels without river flow (no river flushing). In practice, the morphodynamic behavior also depends on the location of the channel within the estuary. Some flood or ebb-dominated channels may show (quasi) morphodynamic equilibrium due to sediment supply from adjacent channels. Furthermore, relatively short tidal inlet channels may behave in a different way than longer estuary channels.

We studied the velocity asymmetry effects in the mouth region of tidal channels based on computed data available in the literature and new additional Delft3D model simulations. The focus is to obtain a simple relationship between tidal velocity asymmetry ($\gamma_a = \hat{\overline{u}}_{flood} / \hat{\overline{u}}_{ebb}$) and the relative tidal amplitude ($\hat{\eta}_o / h_o$), which can be used if the TSAND model is used in stand-alone mode (feasibility studies/quick scan studies), see Fig. 8 and Table 1 with all data sources included. The data refer to computed peak tidal velocities in the mouth of various tidal channel sections of major European rivers based on non-linear 2DH and 3D model results. For almost all natural tidal rivers/channels, the velocity asymmetry is > 1 (flood dominance), but the asymmetry factor remains small between 1 and 1.2. The model simulations for the Ems river (Van Maren et al. 2015b) are based on two Manning coefficients (relatively smooth: $n = 0.01$ or $C = 130\ m^{0.5}/s$; relatively rough: $n = 0.02$ or $C = 65\ m^{0.5}/s$). The upper error bar of the Ems river data (Fig. 8) refers to smooth bed conditions and the lower error bar refers to rough bed conditions. The velocity asymmetry is about 10% larger for smooth bed conditions. The model results of Herrling et al. (2014) for the Ems river show a somewhat smaller asymmetry value.

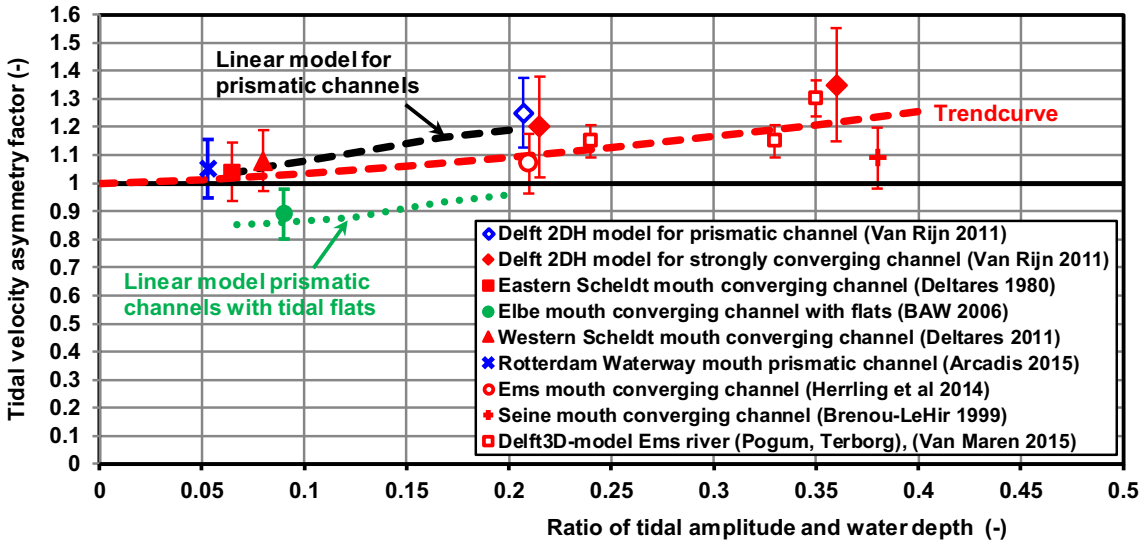

Fig. 8 Effect of relative water depth (ratio of tidal amplitude and water depth) on tidal velocity asymmetry in the mouth region of prismatic and converging tidal channels based on model results

The Elbe tidal channel at Cuxhaven (mouth region) is an exception with a velocity asymmetry factor of 0.9 (Fig. 8), which is most likely related to the presence of wide tidal flats (5 to 10 km wide) in the mouth region. The water volume above the flats drains through the main channel during ebb with relatively small water depths resulting in a strong increase of the peak tidal velocity during ebb. The ratio V_s/V_c is about 1 and $\hat{\eta}_o/h_o$ is about 0.1 which yields ebb dominance based on the results of Friedrichs and Aubrey (1988).

Some results of the linear model are also shown in Fig. 8. A first-order estimation of the tidal asymmetry can be obtained by using the linear model with the same settings at high water

Table 1 Computed peak tidal velocities in various tidal channels based on non-linear 2DH and 3D models

Location	Tidal amplitude (m)	Water depth to MSL (m)	River velocity (m/s)	Peak tidal velocities at mouth (m/s)		Peak tidal velocities at mouth corrected for river velocity(m/s)		Velocity asymmetry (−)
				Flood	Ebb	Flood	Ebb	
Rotterdam Waterway; Hoek van Holland; prismatic (Arcadis 2015)	0.85	16	0.1	0.85	0.95	0.95	0.85	1.05
Westerschelde Vlissingen; converging (Deltares 2011)	2	25	0	1.25	1.15	1.25	1.15	1.08
Oosterschelde converging (Deltares 1980)	1.3	20	0	1.25	1.2	1.25	1.2	1.04
Elbe Cuxhaven converging (BAW 2006)	1.5	16.5	< 0.03	1.6	1.8	1.6	1.8	0.9
Ems Pogum converging (Herrling et al. 2014)	1.5	7	< 0.03	1.4	1.4	1.45	1.35	1.07
Seine Honfleur; converging (Brenou-Le Hir Brenou and Le Hir 1999)	3.5	9	< 0.03	1.9	1.75	1.9	1.75	1.09
Ems river	1.75	7	< 0.05	1.7	1.4	1.7	1.4	1.2
Delft3D model (Van Maren et al. 2015b)	1.65	7		1.3	1.2	1.3	1.2	1.1
	1.85	5		1.5	1.1	1.5	1.1	1.35
	1.85	5		1.05	0.8	1.05	0.8	1.3
Delft2DH model Schematic prismatic channel (Van Rijn 2011a)	2.07	10	0	1.0	0.8	1.0	0.8	1.25
Delft2DH model Schematic converging channel (Van Rijn 2011a)	1.8	5	0	0.95	0.70	0.95	0.70	1.35
	2.15	10	0	0.75	0.63	0.95	0.73	1.20

and at low water. The tidal asymmetry can be expressed as $\gamma_A = c_{max}/c_{min}$ with c_{max} = wave speed at high water and c_{min} = wave speed at low water. As the peak tidal velocity is proportional to the wave speed, see Eq. (5c), it follows that $\gamma_A = c_{max}/c_{min} \cong \hat{\bar{u}}_{flood}/\hat{\bar{u}}_{ebb}$. Very reasonable results can be obtained by defining an effective high water depth and low water depth as $h_{max} \cong h_o + 0.5\hat{\eta}_o$ and $h_{min} \cong h_o - 0.5\hat{\eta}_o$. The linear model has also been applied for a compound channel with a main channel (b_c = 500 m; k_s = 0.1 m) and tidal flats (see Fig. 2) with V_s/V_c in the range of 0.2 to 0.05, yielding an asymmetry factor between 0.85 and 1 (ebb dominance) for $b_{flats}/b_{channel} = 1$. The asymmetry is smallest (0.85) for a deep main channel. The asymmetry is about 0.75 for $b_{flats}/b_{channel} = 4$. The asymmetry factor approaches 1 for a shallow main channel with tidal flats. The flood-related asymmetry for prismatic and converging channels without large-scale tidal flats (trend curve of Fig. 8) can be represented by the following fit: $\gamma_a = 1 + (\hat{\eta}_o/h_o)^{1.5}$. This latter expression (goodness of fit $r^2 \cong 0.4$) is used in the stand-alone TSAND model for the computation of net tide-integrated sand transport rates (Section 4.2). Available field data sets should be studied to confirm the proposed velocity asymmetry relationship, which is mainly based on model data.

3.4 Peak tidal velocities along tidal channels

Channel deepening of a relatively long tidal channel and its effect on sand transport and morphology requires knowledge of the tidal velocities along the entire channel. Information of the horizontal distribution of the peak tidal velocities is essential to understand the erosion and deposition patterns in prismatic and converging tidal channels. We have studied various schematic cases (two types of channels; two channel lengths, and two water depths) to identify patterns of increasing or decreasing velocities along the channel and the effects of channel deepening on this. Non-linear 2DH and 3D models were used to better deal with the channel convergence effects.

The schematic cases are as follows: prismatic and converging channels with lengths of 60 km (<< tidal wave length) and 180 km (≅ 0.5 tidal wave length) and water depths of 5 and 10 m. A rough estimate of the tidal wave lengths ($L = c\,T$) is about 300 km for a depth of 5 m and 450 km for a depth of 10 m. Hence, a channel length of 180 km corresponds roughly to half a tidal wave length. The water depth range of 5 to 10 m represents the interval of regime change from damping to amplification. We have applied a tidal range of 4.2 m (sinusoidal tidal wave at the mouth) and a closed landward boundary (zero discharge); the bed roughness is k_s = 0.05 m.

The horizontal distribution of the peak tidal velocities (flood, ebb) in a short converging tidal channel with length of 60 km based on non-linear Delft3D model results (2DH mode) is shown in Fig. 9. The width at the mouth is 25 km and the width at the closed end is about 2 km (convergence length scale of about 25 km; strongly converging channel). Wave reflection can be clearly observed at the landward end of the channel (x = 40–55 km) for a depth of 5 m, see tidal range of Fig. 9.

The peak flood velocity is of the order of 1 ± 0.25 m/s and remains fairly constant up to 25 km from the mouth. It takes about 15 km for the sinusoidal wave to adjust to an asymmetric shoaling tidal wave. The computed peak ebb velocity gradually decreases in landward direction. If the water depth is 10 m, the tidal range is amplified but the computed peak flood velocity remains fairly constant at a value of 0.75 m/s up to 25 km from the mouth and decreases gradually after that. If the water depth is 5 m and tidal damping is dominant, the peak tidal velocity decreases in landward direction of the converging channel (x > 30 km).

Figure 9 also shows computed peak velocities (mean of two computations) in the converging Ems river in Germany based on the Delft3D model simulations with Manning coefficient n = 0.01 to 0.02 (Chézy = $h^{1/6}/n$ ≅ 130 to 65 $m^{0.5}/s$), bathymetry of 2005, and depths of 5 to 7 m (Van Maren et al. 2015b). A weir is present at Herbrum (15 km upstream of Papenburg; 85 km from mouth) where the measured discharge rate is used as landward boundary condition. The tidal range (at spring tide) shows an increase from about H_o = 2.8 m at the model boundary Elmshorn to about 3.1 m in Knock (20 km), about 3.4 m in Pogum (35 km), to about 3.6 m in Papenburg at 70 km. Hence, the tide is strongly amplified due to geometry effects and resonance effects (upstream weir). The computed peak tidal velocities are gradually decreasing from stations Pogum to Papenburg (Van Maren et al. 2015b). The peak velocities in the sections Knock to Pogum (20–35 km) of the Ems river are relatively large (up to 1.5 m/s) due to the presence of a long funnel type training wall with groins (transition from estuary to river). The computed peak tidal velocities in the river mouth section between 35 and 60 km show a slightly decreasing trend. These qualitative trends have also been found by Chernetsky et al. (2010) for the Ems river.

Similar computations have been made for a long converging channel of 180 km (schematic case), see Fig. 10. The flow width of the converging channel decreases from 25,000 m at the mouth to 10 m at the closed end (strongly converging channel with convergence length scale of about 25 km). Tidal damping is present in the converging channel with water depth of 5 m; the tidal range decreases from 4.2 m at the mouth to about 3 m at the end. Wave reflection is present at the end of the channel (150–180 km) where the tidal range is relatively large (not shown) for both depths (5 and 10 m). The peak flood velocity near the mouth (< 25 km) remains fairly constant at 0.9 ± 0.2 m/s. The peak ebb velocity is somewhat smaller (not shown). Strong tidal amplification of the tidal range is present for a converging channel with h = 10 m; the tidal range increases from 4.2 m at the mouth to about 9 m at the end. The peak flood velocity gradually increases from

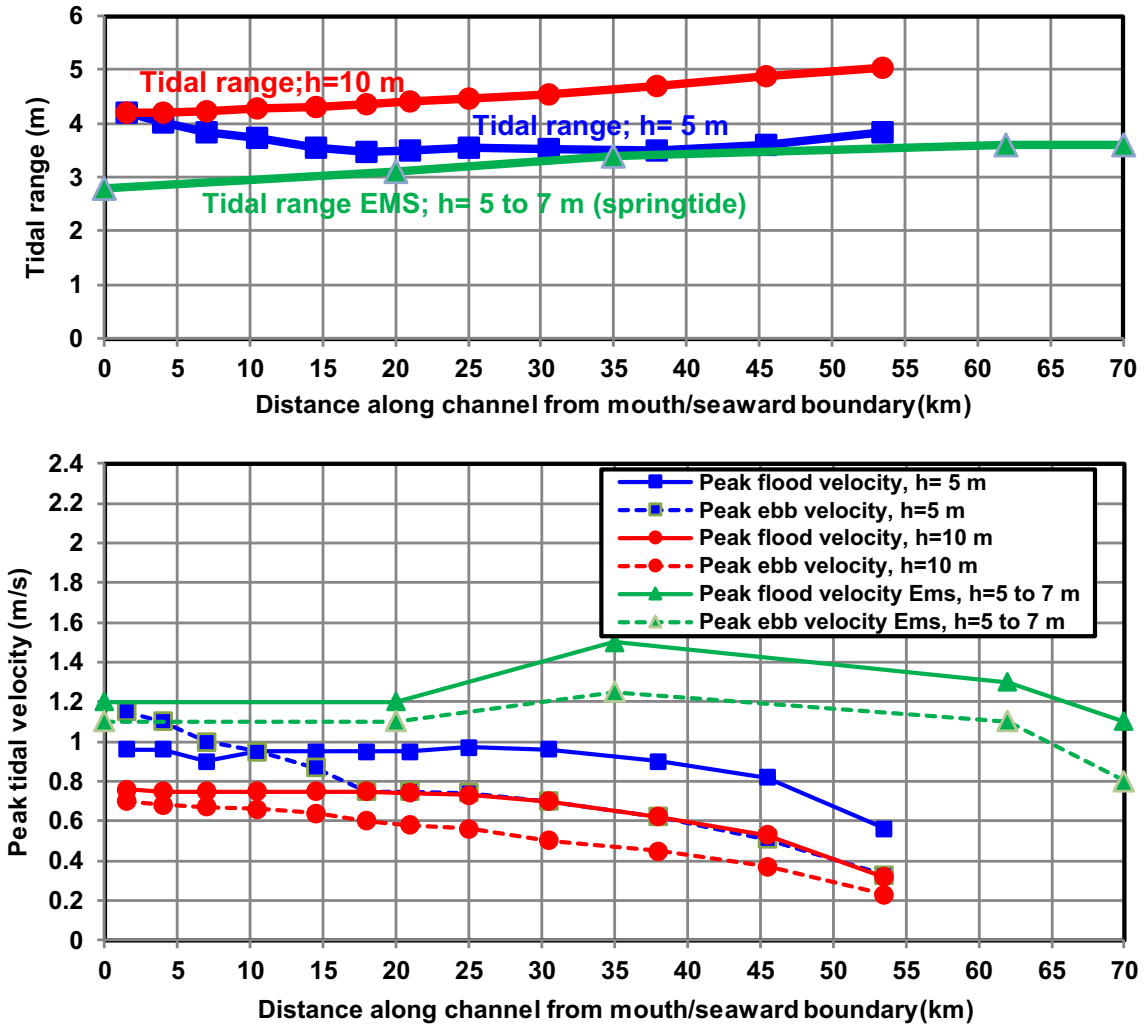

Fig. 9 Effect of water depth on tidal range (upper) and peak flood and ebb velocities (lower) in short converging channels based on non-linear 2DH and 3D-models

0.8 m/s at the mouth to 1.4 m/s near the end. Similarly, the peak ebb velocities increase from about 0.8 m/s at the mouth to about 1.25 m/s near the end (not shown). Hence, the peak tidal velocities are increasing in a strongly converging tidal channel (strong amplification) with a water depth of 10 m, particularly beyond the mouth region (> 30 km). It is noted that a convergent channel reducing to a width of about 10 m over a distance of 180 km is not very realistic in practice. It is more likely that after a convergent section, the river has a constant width. This case, which has also been studied (Van Rijn 2011a), shows that damping due to bottom friction is the dominant process in the constant width section.

In the prismatic channel with a length of 180 km, the peak tidal velocity always decreases in landward direction due to the tidal damping effect. The decrease of the velocity is less for a larger water depth (less damping), as shown in Fig. 10.

The effect of channel deepening on the peak tidal velocities in the prismatic Rotterdam Waterway is presented in Fig. 11 based on results of the non-linear 3D model including salinity. The depth-averaged peak flood current velocity is about 0.8 m/s in the wider outer section and increases to about 1.2 m/s in the narrower section (1030–1015 km). The velocity is largest in the opening of the Maeslant barrier where the river width is smallest. The velocity reduces to about 0.8 m/s in the upstream river sections.

Figure 11 makes clear that the further deepening of an already deep channel from 15 to 16.3 m such as the Rotterdam Waterway (from 15 to 16.3 m) only has a marginal effect on the depth-averaged velocities (lowest panel of Fig. 11). This was also concluded by DiLorenzo et al. (1993) for the Delaware estuary (USA). However, the 3D model results of the Rotterdam Waterway show that the near-bed flood velocities are most significantly affected (variation of 20%) in the section 1020–1010 km with the salinity front, which has serious consequences for the sand transport and deposition processes in that region.

Summarizing, channel deepening in a prismatic channel leads to less tidal damping and hence to slightly larger tidal

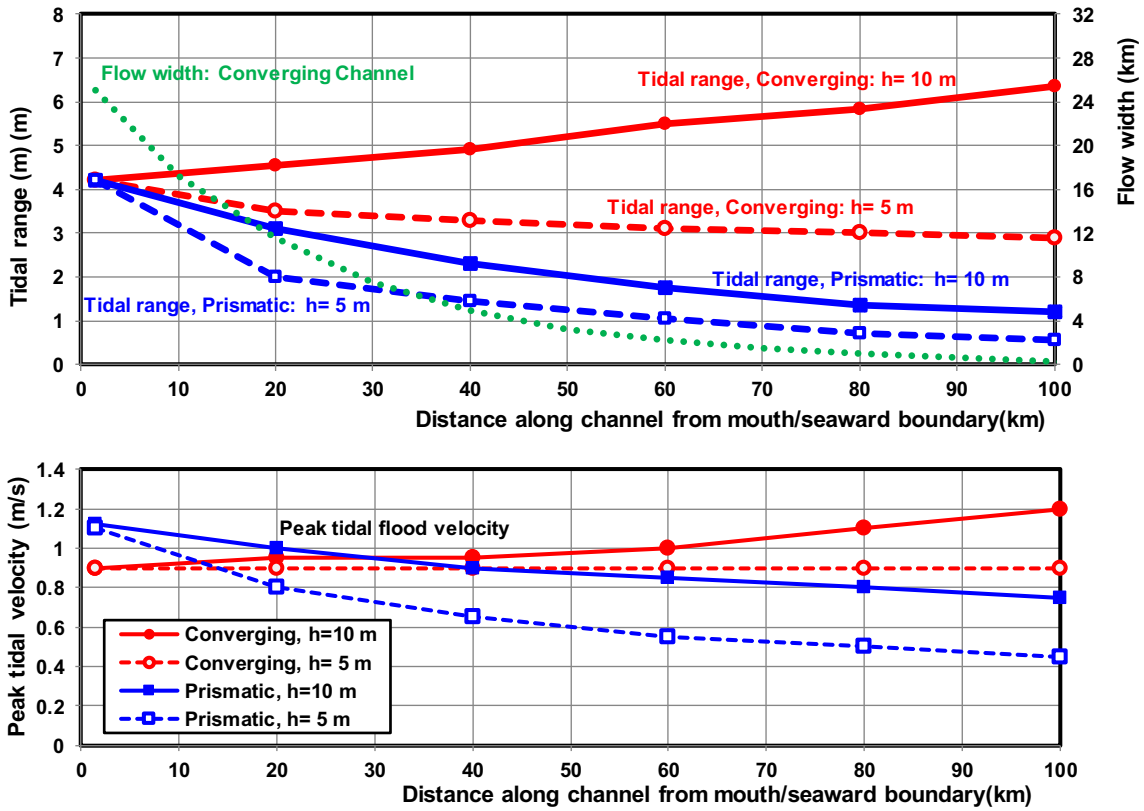

Fig. 10 Effect of water depth on tidal range (upper) and peak flood velocities (lower) in long, converging/prismatic channels (180 km) based on non-linear 2DH model

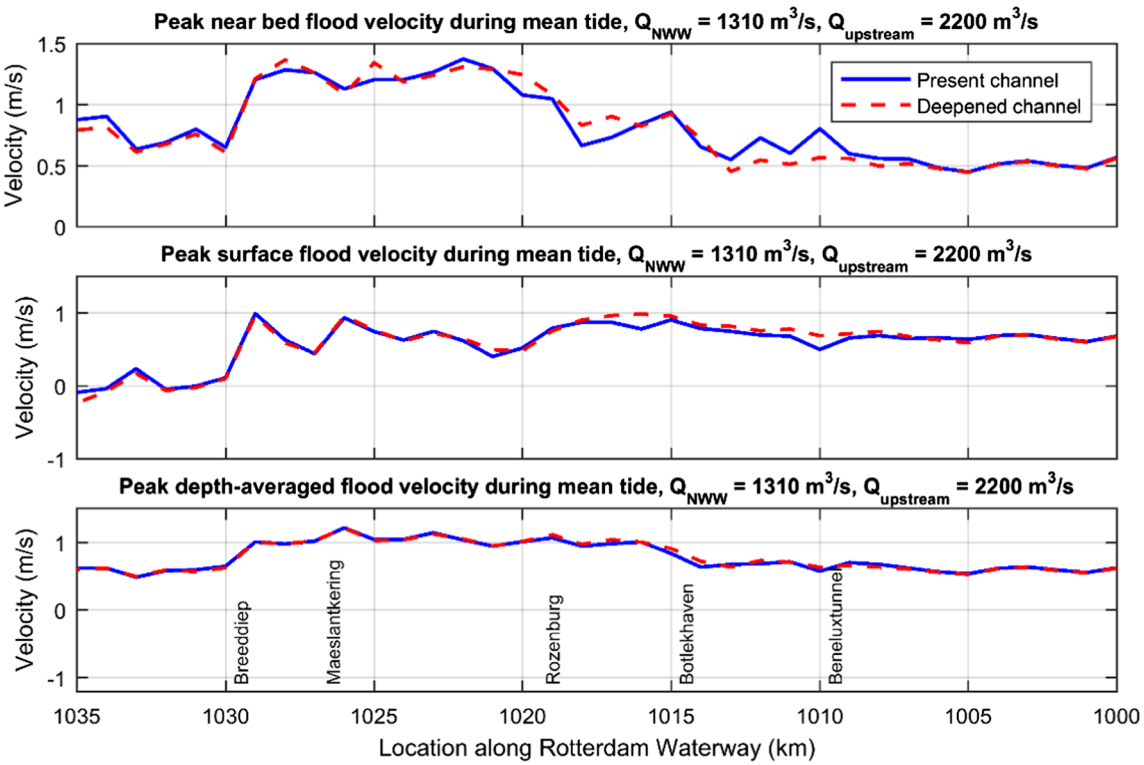

Fig. 11 Effect of water depth on peak flood velocities along Rotterdam Waterway for present and deepened channel (North Sea at 1035 km) based on non-linear 3D model; tidal range H_o = 1.85 m and $Q_{waterway,50\%}$ = 1310 m³/s ($Q_{Lobith\ upstream,\ 50\%}$ = 2200 m³/s) (Arcadis 2015)

ranges. The peak tidal velocity in a deepened prismatic channel remains fairly constant in the mouth region. Further deepening of an already deep channel only has a marginal effect on the depth-averaged velocities. However, near-bed velocities may be significantly (about 20%) affected in the salinity front zone.

Channel deepening from a small depth of about 5 m to a larger depth of 10 m in a strongly converging channel leads to a regime shift from tidal damping to tidal amplification with much larger tidal ranges along the channel. Similar results have been found by DiLorenzo et al. (1993), Chernetsky et al. (2010), Winterwerp (2011), Van Maren et al. (2015a, b), and Familkhalili and Talke (2016). The peak tidal velocities in the mouth region (< 25 km) of a converging channel may decrease by about 20% due to channel deepening. The present cases studied using linear and non-linear models do not show any significant increase of the peak tidal velocities in the mouth region due to channel deepening in converging channels.

Our results substantiate earlier ideas of Friedrichs (2010), who has observed that many prismatic and converging tidal channels with an erodible sediment bed have a rather constant peak tidal velocity in the mouth region and are typified as "equilibrium" to "near-equilibrium" channels.

In the following Section 4, it is studied how the tide-integrated sand transport processes are affected by channel deepening in the prismatic tidal channel of the Rotterdam Waterway. As a result, the depth of a near-equilibrium tidal channel with an erodible sediment bed is more precisely defined.

4 Effect of channel deepening on tide-integrated sand transport along tidal channels

Hereafter, in Section 4.1, the effect of channel deepening on the sand transport processes in the Roterdam Waterway is studied using a detailed 3D model in combination with the TSAND model. The detailed 3D model of the Rotterdam Waterway is based on very small grid cells resulting in relatively large run times. To be able to do many sensitivity sand transport runs, the 3D model output of the near-bed velocity and salinity values along the channel axis during the neap-spring tidal cycle is used as input for the TSAND model. Many runs were made to determine mean values including the variation range of the net sand transport rates along the channel axis, which could not have been done by using the 3D model including the advection-diffusion equation of the sand concentrations and transport rates. First, it is shown that the TSAND model produces sand transport rates which are in good agreement (justification) with those of the detailed Delft3D model. After that, the results of some sensitivity runs varying the most influential parameters are shown and discussed.

In Section 4.2, the TSAND model is used in stand-alone mode with hydrodynamic input results from Section 3 to compute the net tide-integrated sand transport rates for a wide range of water depths and freshwater discharges in order to explain the change from sand export to import and the concept of equilibrium depth of tidal channels.

Finally, in Section 4.3, the results are discussed.

4.1 Channel deepening of Rotterdam Waterway: 3D model with TSAND

We have validated the TSAND model in post-processing mode (with hydrodynamic input of the 3D model) by comparing the sand transport rates of the 3D model (10 vertical grid points) with and without the TSAND model. The channel bed consists of sand with $d_{50} = 0.25$ mm and mud with varying percentages of 5% at the mouth to 35% near Rotterdam. Local patches of gravel are present as relict features of local bed stabilization measures. The d_{50} of the sand fraction is varied in the range of 0.15 to 0.35 mm based on observed values.

The boundary conditions are a spring-neap tidal cycle (tidal range of about $H = 2$ m) in combination with a freshwater discharge in the Waterway of $Q_{\text{waterway},50\%} = 1310$ m^3/s. Using default parameter settings, the TSAND model with 50 grid points over the water depth and near-bed velocity input of the 3D model (including salinity effects) produces very similar sand transport results as that of the 3D model with advection-diffusion equation for sand concentrations, see Fig. 12. The net tide-integrated sand transport is obtained by integrating the instantaneous sand transport rates over the spring-neap cycle and dividing by the number of tides within the cycle and is expressed in ton per meter per tide. The differences between the 3D model and the TSAND model are largest (maximum 55%) in the mouth region (1030–1027 km). These deviations are mainly caused by the difference in the number of vertical grid points used in both models (10 points in 3D model and 50 points in TSAND model).

Many TSAND post-processing runs were done varying the most important sand transport parameters and model coefficients (Arcadis 2015). The focus parameter is the net tide-integrated sand transport rate, which is shown in Fig. 13 for springtide in combination with five freshwater discharges and $d_{50} = 0.15$ mm.

The tide-integrated sand transport rate is landward-directed at all locations except for the largest freshwater discharge of $Q_{95\%} = 2500$ m^3/s in the waterway. In the latter case, the transport rate is in landward direction between 1035 and 1020 km and seaward beyond 1020 km. It is noted that the net sand transport rate upstream in the region of Rotterdam ($x <$ 1010 km) is almost zero due to the presence of relatively small depth-averaged flow velocities during the tidal cycle (< 0.6 m/s),

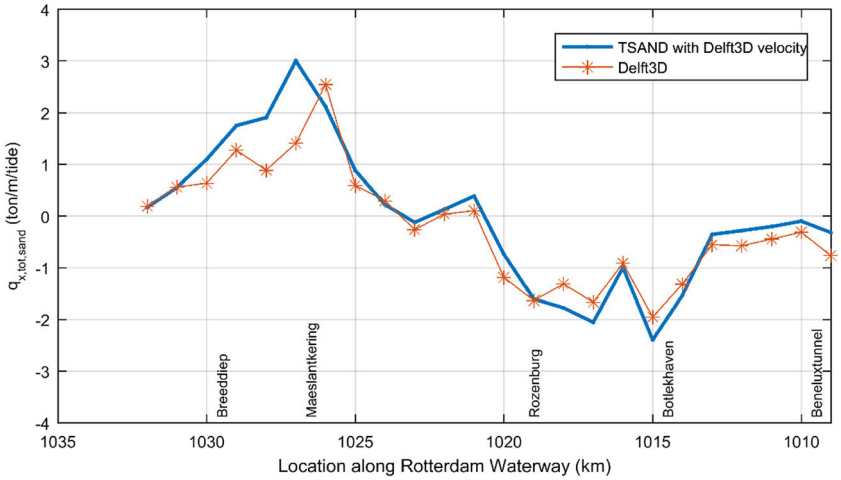

Fig. 12 Comparison of net tide-integrated sand transport (+ landward) along the Rotterdam Waterway (North Sea at 1035 km) based on 3D model; neap-spring cycle; river discharge $Q_{waterway,50\%} = 1310$ m^3/s; $d_{50} = 0.25$ mm (Arcadis 2015)

even at large freshwater discharges. The sand transport far upstream in the almost steady river flow section is about 10 to 20 ton/m/tide. Sand is mined/dredged in the depositional area at the transition between the tide-dominated and river-dominated sections.

The dominant effect of the flood velocities on the net tide-integrated sand transport rates can be explained by Fig. 14, which shows the velocity, salinity, and sand concentration profiles during peak flood and ebb flow at 1030 km during mean tide, freshwater discharge $Q_{waterway,50\%} = 1310$ m^3/s and $d_{50} = 0.25$ mm. The velocity and salinity profiles are from the 3D model, whereas the sand concentration profiles are from the TSAND model. During flood tide, the near-bed velocities are relatively large due to the presence of strong horizontal salinity gradients driving the water in landward direction. The near-surface flood velocities are strongly reduced by the freshwater discharge. During ebb tide, the near-bed velocities are relatively small as the salinity gradient opposes the ebb flow. The near-surface ebb velocities are large with values of up to 2 m/s. The salinity values are largest during flood tide, particularly in the upper half of the water column. The sand concentrations are largest during flood tide due to the relatively large near-bed velocities. The sand concentrations during ebb flow are extremely small (almost zero with values < 5 mg/l). The near-bed velocities and associated bed-shear stresses during ebb tide are too small to generate significant sand transport, which explains the strong flood dominance of the tide-integrated sand transport.

The effect of grain size is presented in Fig. 15 for $d_{50} = 0.15$, 0.25, and 0.35 mm based on the weighted average of 15 runs (3 tides: spring, mean, and neap tide; 5 freshwater discharges: $Q_{5\%}$, $Q_{25\%}$, $Q_{50\%}$, $Q_{75\%}$, and $Q_{95\%}$). It was found that the weighted average values can be best represented (not shown) by the $Q_{75\%}$ value. The net tide-integrated sand transport is landward at all locations between the mouth (1035 km) and the city of Rotterdam (1010 km). The transport rates are largest for fine sand of 0.15 mm and smallest for sand of 0.35 mm. Based on the results of Figs. 13 and 15, the import of sand at the mouth at 1035 km is about 1.5 ± 0.75 ton/m/tide for water depths in the range of 10 and 15 m and freshwater discharge of $Q_{50\%} = 1310$ m^3/s or about 2.5 m^2/s (river width of about 500 m).

Analysis of dredging volumes of the southern part of the mouth channel yields an annual value of about

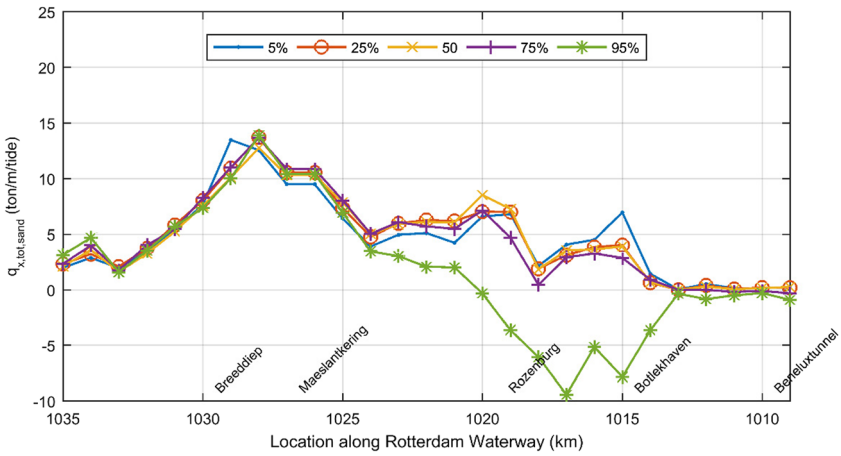

Fig. 13 Effect of river discharge on net tide-integrated sand transport (+ landward) in present situation (North Sea at 1035 km) based on TSAND model; springtide; $Q_{waterway,5\%} = 480$, $Q_{25\%} = 1010$, $Q_{50\%} = 1310$, $Q_{75\%} = 1670$, $Q_{95\%} = 2500$ m^3/s; $d_{50} = 0.15$ mm (Arcadis 2015)

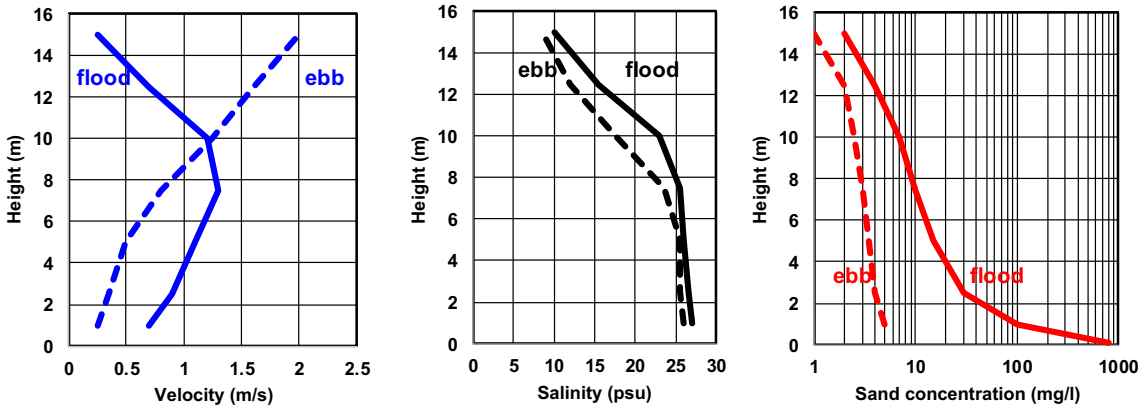

Fig. 14 Computed velocity, salinity, and sand concentration profiles (3D model) for maximum flood and ebb flow at 1030 km (near the mouth) in present situation, mean tide, and river discharge $Q_{\text{waterway},50\%} = 1310$ m^3/s, $d_{50} = 0.25$ mm (Arcadis 2015)

1 ± 0.5 million m^3 (Arcadis 2015). Using an effective width of 500 m, a bulk density of 1.5 ton/m^3, and 730 tides per year, the sand import at the mouth is about 4 ± 2 ton/m/tide, which is larger than the computed value of 1.5 ± 0.75 ton/m/tide. The higher sand import values based on the dredging records can be explained by the presence of surface waves in the mouth which leads to larger suspended transport rates and to more import of sand (in the winter season). Surface waves were not simulated in the model runs.

Figures 13 and 15 show that the tide-integrated sand transport is highest at 1028 km which is just upstream of the Maeslant tidal barrier where the channel width is smallest resulting in relatively large flow velocities. The increase of the tide-integrated transport rate from the mouth to the barrier location means erosion of the order of 2 ton/m/tide for $d_{50} =$ 250 μm. Using a river width of 500 m, a bulk density of 1.5 ton/m^3, and 730 tides per year, the erosion volume is about $500 \times 2 \times 730/1.5 = 0.5$ million m^3/year over a section with length of 8000 m and width of 500 m. This yields an erosion depth of about 0.1 m/year. In reality, the northern mouth section is gradually deepening (about 0.05 m per year; Arcadis 2015) with some dredging locally. Hence, the net tide-integrated sand transport rates in this section are overestimated, which is most likely caused by cohesive effects due to the presence of mud (about 5 to 35%).

Landward of the tidal barrier (1027 km), the tide-integrated sand transport decreases to almost zero at 1015 km which means deposition in this channel section of the order of 0.5 million m^3/year (similar to the erosion volume). The annual dredging volume of mainly sand in this section is of the order of 0.3 to 0.5 million m^3/year (Arcadis 2015).

Overall, it can be concluded that the trends of erosion and deposition along the sandy channel bed are correctly represented but the values are somewhat overestimated by the TSAND model using the hydrodynamics of the 3D model as input.

Finally, the effect of a planform realignment at 1030 km and the channel deepening (from 15 m to 16.3 m below mean sea level between 1030 and 1010 km) on the tide-integrated transport of sand with $d_{50} = 0.25$ mm is shown in Fig. 16. The effect of a planform realignment at 1030 km leads to significant changes of the flow velocities and hence the tide-integrated sand transport rates on both sides of the realignment location. The flow velocities and sand transport rates decrease between 1033 and 1030 km and increase between 1030 and 1027 km. These effects are temporary effects as the alluvial

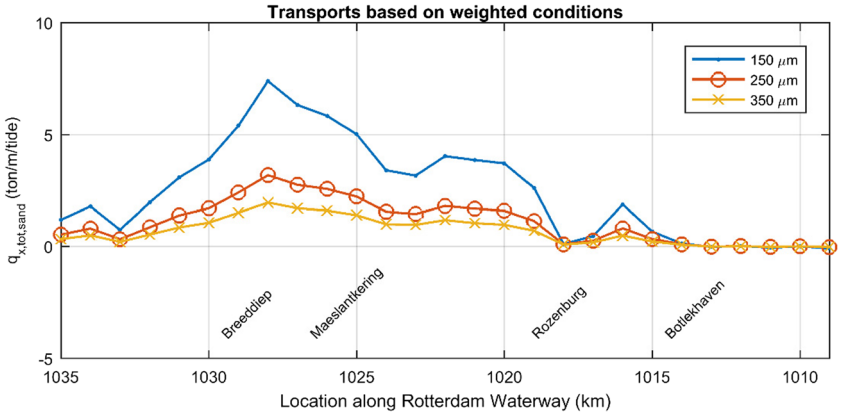

Fig. 15 Effect of sand grain diameter on net tide-integrated sand transport (+ landward) in present situation (North Sea 1035 km) based on TSAND model; weighted average for all conditions (five river discharges, three tide neaps, mean, spring) (Arcadis 2015)

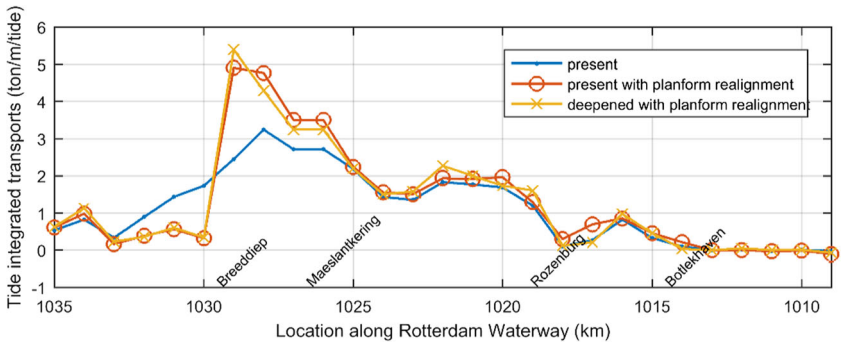

Fig. 16 Effect of water depth and planform on net tide-integrated sand transport for new situation (North Sea 1035 km) based on TSAND model; weighted average for all conditions (five river discharges, three tide neaps, mean, spring); $d_{50} = 0.25$ mm (Arcadis 2015)

bed will adjust locally to a new equilibrium bed level. The effects of channel deepening are only marginal with variations (with respect to the planform effect) of about 10 to 15%.

4.2 Channel deepening at mouth of tidal channels (schematic cases): stand-alone TSAND model

An important question related to channel deepening is the risk of regime change in the mouth region from import to export or vice versa. To be able to compute the net sand transport over a large range of conditions, we have used the simplified TSAND model in stand-alone mode (with hydrodynamic data of the linear model from Section 3) for a prismatic tidal channel (without tidal flats). The model including tidal flow, river flow, salinity circulation, and sand transport is used for sand with $d_{50} = 0.25$ mm and water depths between 5 and 20 m. The tidal range is 2 m.

The results of Section 3 show that the tidal velocities decrease slightly for increasing water depth in the case of prismatic channels. The 3D tidal model used for the prismatic Rotterdam Waterway shows that the peak tidal depth-averaged velocities remain about the same if the water depth is increased by about 10% (Fig. 11). Van Maren et al. (2015a) have found for the converging Ems tidal channel that the bed-shear stresses and hence the velocities along the channel are not much affected by a considerable increase of the water depth (bathymetry of 2005 instead of 1985; their Fig. 11) for the converging Ems-Dollard estuary.

Given these results, it is reasonable to assume that the peak tidal velocity in the mouth region of a tidal channel is approximately constant (at about 1 m/s) for a range of water depths between 5 and 20 m in prismatic and weakly converging channels (see also Friedrichs 2010).

The velocity asymmetry ($\overline{u}_{\mathrm{max,flood}}$ /$\overline{u}_{\mathrm{max,ebb}}$) is taken as 1.15, 1.1, 1.08, and 1.05 for depths of 5, 10, 15, and 20 m ($\eta_o/h_o = 0.2, 0.1, 0.067$, and 0.05; $\eta_o = 1$ m = tidal amplitude at mouth, h_o = water depth at mouth) based on Fig. 8. The freshwater river discharge per unit width is varied between $q_r = 0$ and 10 m^2/s. The horizontal density gradient is an input parameter of the TSAND model (stand-alone mode) and is varied between 0.02 kg/m^3/m for a small depth (short intrusion distance) of 5 m and 0.0003 for a depth of 20 m (long intrusion distance) based on available data from the prismatic Rotterdam Waterway (Arcadis 2015).

The focus point of this section is the value of the computed net tide-integrated sand transport as function of the water depth and the river discharge, see Figs. 17 and 18.

The net tide-integrated transport rate clearly decreases for increasing water depth, particularly for depths in the range of 5 to 15 m. For very small river discharges ($q_r < 1$ m^2/s), the net tide-integrated transport rate of sand is landward (import/flood-dominant). At zero river discharge ($q_r = 0$), the net transport rate at the mouth is landward and decreases from about 5 to 1 ton/m/tide for increasing water depths from 5 to 20 m. The net transport rate of sand increases significantly for increasing peak tidal velocity ($\overline{u}_{\mathrm{max}}$ from 0.8 to 1.3 m/s, $h = 10$ m), see Fig. 18. The computed trends show increasing seaward transport for larger river discharges and decreasing seaward transport rates in deeper water (smaller bed-shear stress, see Fig. 20). Each data point has a vertical error bar of at least 50% which is mainly determined by the input value of the horizontal salinity gradient.

Comparison of the transport rates with tidal flow ($\overline{u}_{\mathrm{max}} =$ 1 m/s) and without tidal flow ($\overline{u}_{\mathrm{max}} = 0$) at a depth of 5 m (Fig. 17) shows that the net transport rate increases considerably due to the presence of the tide. This will result in erosion of the tidal region, which is the reason that this region generally is deeper than further upstream (gradually increasing water depth in seaward direction). An equilibrium depth can be defined for prismatic and/or weakly converging tidal channels. The equilibrium depth is the depth at which the net tide-integrated sediment transport is equal to the sediment transport in the steady upstream river flow. For example, the equilibrium water depth is about 10 m for a river discharge of about 4.5 m^2/s (intersection point of dotted curve for upstream river flow with $h = 5$ m and the square-symbol curve for tidal flow with $h = 10$ m, see Fig. 17).

Based on Fig. 17, the net landward tide-integrated transport rates for low river discharges (< 2 m^2/s) are of the order of 1 to 3 ton/m/tide (2 ± 1) for water depths between 5 and 20 m. These values are in reasonable agreement with the computed values (3D model) of Figs. 13 and 15 for the Rotterdam Waterway yielding a slightly smaller import value of 1.5 ± 0.75 ton/m/tide

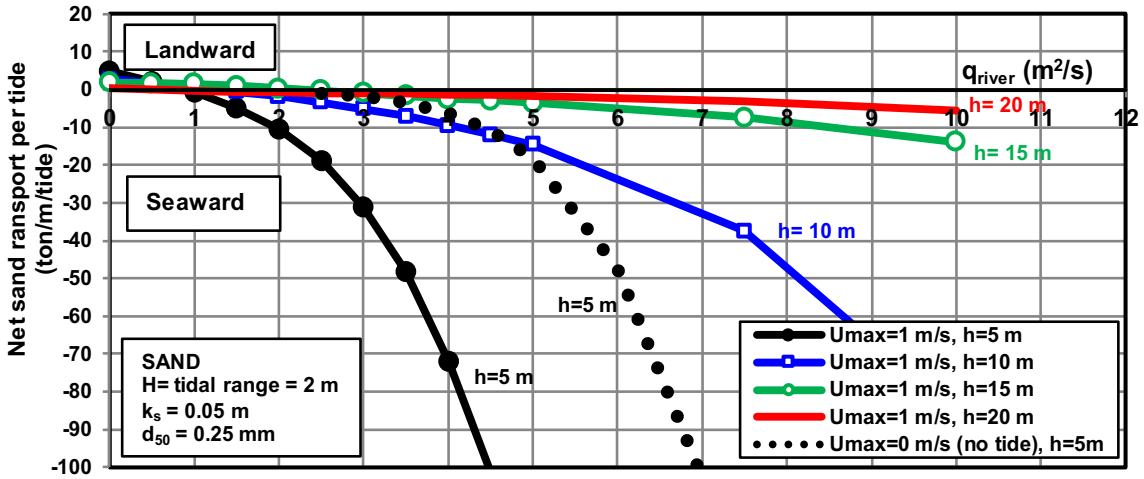

Fig. 17 Effect of water depth and river discharge on net tide integrated sand transport at mouth of prismatic channel; TSAND model

at the mouth (1035 km). It is noted that the computed values are somewhat smaller than the observed sand import of about 4 ± 2 million m^3/year at the mouth (based on dredging records; Arcadis 2015). A possible cause for the underprediction is the absence of the effect of surface waves on the sand transport rates in Fig. 17. Surface waves enhancing suspended transport and sand import are present in the mouth region of the Rotterdam Waterway, particularly in the winter season.

Using a channel width of 500 m, a net import of 2 ton/m/tide, and a bulk density of 1.5 ton/m^3, the annual volumetric import of sand based on 730 tides is $500 \times 2 \times 730/1.5 \cong 0.5$ million m^3/year, which is a small quantity for a wide tidal river. Further deepening by dredging of an already deep channel (from 15 to 20 m) to accommodate larger vessels will lead to a small reduction of the import (decreasing import of sand of 10 to 20% for increasing depths at low river discharges).

A remarkable phenomenon of Fig. 17 is the ebb dominance of the prismatic channel system in the case of a significant river flow discharge > 2 m^2/s. This can be explained by Fig. 19, which shows computed velocity and sand concentration profiles at peak flood and ebb flow for a depth of 10 m, q_r = 3 m^2/s, and $\overline{u}_{max}$ = 1 m/s using both the single and multi-fraction methods. The sand concentrations during ebb flow are much larger than during flood flow conditions (ebb dominance). The single fraction results are based on the assumption that the suspended sediment size is equal to the bed material size ($d_{sus} = d_{50}$). The results clearly show that the near-bed velocities during flood are relatively large due to the presence of horizontal salinity gradients. During ebb flow, the near-surface velocities are relatively high (freshwater outflow). The multi-fraction method yields relatively large sand concentrations in the upper part of the water column due to the presence of the fine sand fractions. Sensitivity computations for $d_{50} = 0.15$ mm (finer sand) and 0.35 mm (coarser sand) show that the net transport rate increases by about a factor of 2.5 for d_{50} = 0.15 mm and decreases by a factor of 2 for $d_{50} = 0.35$ mm.

Another phenomenon is the decrease of the net transport rate for increasing water depth, which can be explained by Fig. 20. This shows the peak bed-shear stresses during flood and ebb flow as function of the ratio with $\overline{u}_r / \overline{u}_{max}$ with $\overline{u}_{max}$ =

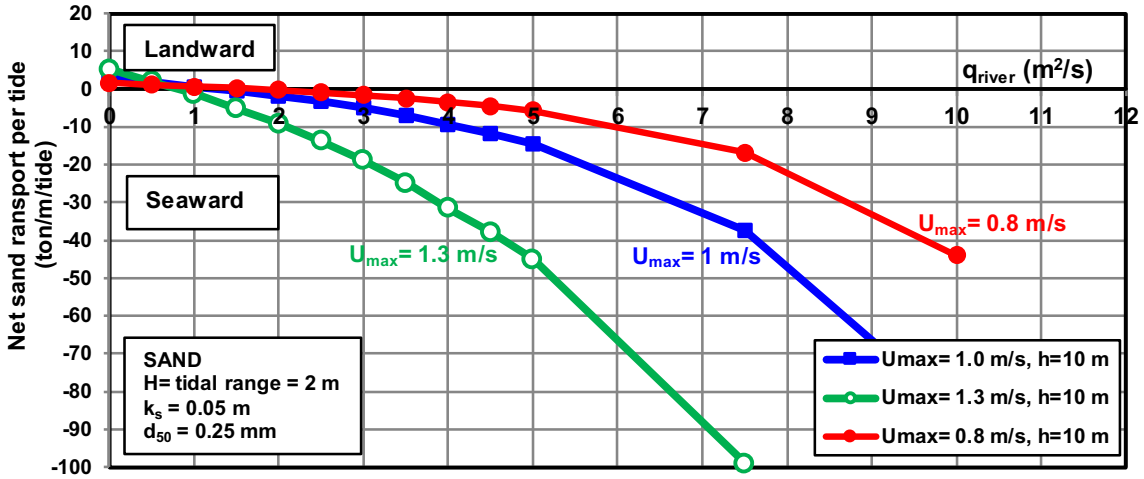

Fig. 18 Effect of peak tidal velocity and river discharge on net tide integrated sand transport at mouth of prismatic channel; TSAND model

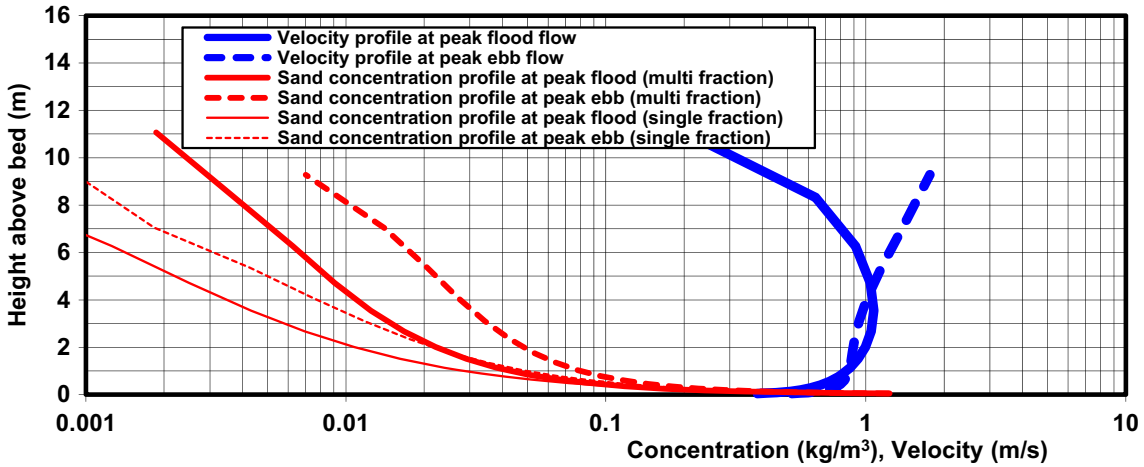

Fig. 19 Computed velocity and sand concentration profiles at peak flood, ebb velocity for $h = 10$ m, $q_r = 3$ m^2/s, $\bar{u}_{max} = 1$ m/s; TSAND model

1 m/s. The peak flood bed-shear stresses decrease for increasing river discharges, whereas the peak ebb bed-shear stress increase for increasing river discharges. At low river discharges, both the peak flood and the peak ebb bed-shear stress decrease for increasing water depth.

4.3 Discussion

The consequences of the results of Figs. 17, 18, 19, and 20 can be best explained by an example of a prismatic tidal channel with a sandy bed such as the Rotterdam Waterway. For this purpose, we consider two fixed locations: upstream river section (no tide) and downstream tidal mouth region, both with an equal water depth of 5 m. The upstream sand transport for a depth of 5 m and a river discharge of 4.5 m^2/s (river velocity of 0.9 m/s; Rhine river) is about 12 ton/m/tide (export to the sea; Fig. 17). The sand export in the tidal mouth region at a depth of 5 m, and at the same river, discharge of 4.5 m^2/s is about 100 ton/m/tide (Fig. 17). Thus, the net transport rate in the tidal channel section (with depth of 5 m) increases considerably (from 12 to 100 ton/m/tide) due to the presence of tide-induced and salinity-induced flows resulting in erosion. At a water depth of about 10 m in the mouth region, the net transport rate is about equal to 12 ton/m/tide (export) being the transport rate of the upstream river section (with depth of 5 m). Thus, a water depth of 10 m can be seen as the equilibrium water depth of the tidal channel in the mouth region. This example shows that the depths of the tide-influenced sections need to be much larger than the depths of the more inland sections to obtain quasi-equilibrium conditions with a constant transport rate along the channel. The water depths along the tidal section of the river will gradually (exponentially) increase in seaward direction to the equilibrium water depth of 10 m at the mouth.

For water depths smaller than the equilibrium depth, erosion will occur until the depth is equal to the equilibrium depth.

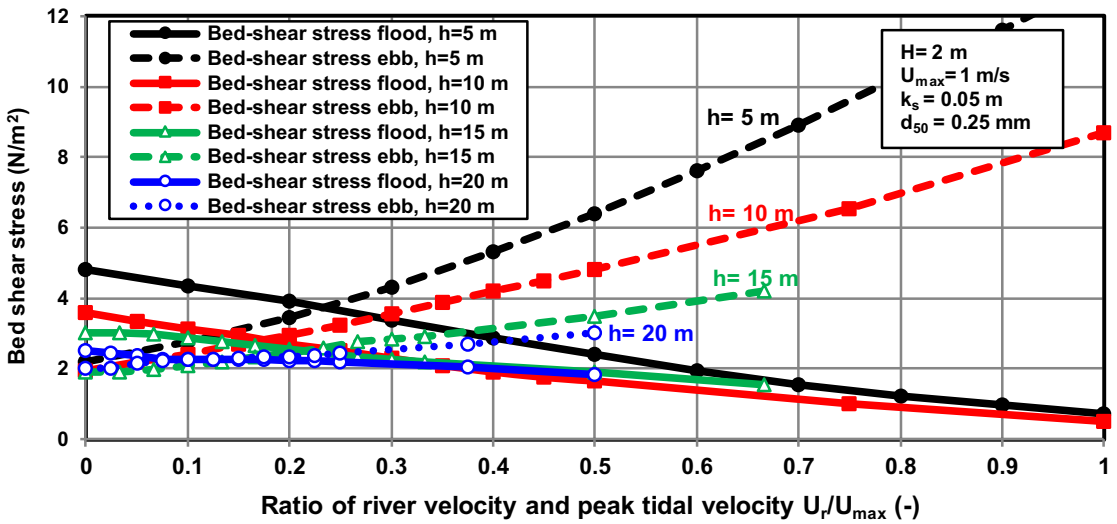

Fig. 20 Effect of water depth and river velocity on computed bed-shear stress at peak flood and ebb velocity for a prismatic channel (no flats); TSAND model

For water depths larger (due to dredging) than the equilibrium depth, deposition will dominate in the tidal section (regime shift from erosion to deposition). If the channel banks are erodible (no dikes or groins), both the width and depth of the channel will adjust to form a converging tidal channel.

Around 1900, the water depth of the Rotterdam Waterway was about 8 to 10 m, which could be maintained without dredging except for the mouth region with sand deposition in the jetty opening (Staatscommissie 1920). Thus, a water depth of 8 to 10 m can be seen as the equilibrium depth of the Rotterdam Waterway in a regime with export of sand for discharges of about 3 m^2/s (see Fig. 17).

For navigational purposes, it is often required to have a relatively deep tidal channel with constant water depth. Based on Fig. 17 (sandy bed), the net transport rate will decrease for larger depths than the "equilibrium" depth resulting in channel deposition. For example, if $h = 15$ m, $q_r = 4.5$ m^2/s, and $\overline{u}_{max} = 1$ m/s, it follows that $q_{s,net} \cong 2$ ton/m/tide (export). This latter value is much smaller (factor 6) than the net transport of 12 ton/m/tide (export) in the upstream river-dominated section where the depth is 5 m. The difference of 10 ton/m/tide will be deposited in the deeper tidal channel (15 m). Using a channel width of 500 m, 730 tides per year, and a bulk density of 1.5 ton/m^3, the deposition volume (mainly river sediments) will be about $10 \times 500 \times 730/1.5 \cong 2.5$ million m^3/year.

This example shows that channel deepening in a prismatic channel beyond the equilibrium depth will always result in significant deposition and associated dredging in the tidal section. Further deepening of an already deep channel from 15 to 20 m only leads to a marginal increase of the deposition volume as the net tide-integrated transport rate (export) at the mouth decreases from about 2 to 1 ton/m/tide, which is equivalent with an additional deposition volume of about 0.25 million m^3/year for a channel of 500 m wide.

5 Conclusions

In this paper, we have identified and discussed the basic processes influencing the sand transport processes in tidal channels. We presented a simplified model for tide- and density-driven currents and resulting sand transport rates and verified these with field data of the Rotterdam Waterway. The advantage of the simplified TSAND model is the rapid assessment of the net tide-integrated sand transport (import or export) at locations in the mouth region of a tidal channel for a range of hydrodynamic and sediment conditions including storm events (sensitivity studies). The simplified TSAND model is a powerful tool to determine the most influential processes and parameters so that the number of detailed 2DH or 3D model runs can be reduced.

The most important findings of the present study are:

1. Channel deepening of a prismatic channel (Rotterdam Waterway) from 10 to 20 m leads to less tidal damping, slightly larger tidal ranges (< 10%), and slightly larger peak tidal velocities (< 10%) in mouth region (< 25 km).
2. Channel deepening from a small depth of about 5 m to a larger depth of 10 m in strongly converging channels may lead to a regime shift from tidal damping to tidal amplification with a much larger tidal range; the peak tidal velocities in the mouth region (< 25 km) remain fairly constant.
3. The tidal velocity asymmetry values in the mouth of a tidal channel are in the range of 1 and 1.2 (flood dominance) depending on the ratio of the tidal amplitude and the water depth for natural tidal channels with no or minor intertidal flats.
4. The net tide-integrated sand transport of sandy tidal channels can be determined with sufficient accuracy by the simplified TSAND model coupled to 1D, 2DH, or 3D hydrodynamic models.
5. Based on the results of the simplified sand transport model, an equilibrium depth can be defined for prismatic and/or weakly converging tidal channels; the equilibrium depth is the depth at which the net tide-integrated sediment transport is equal to the sediment transport in the steady upstream river flow.
6. The equilibrium depth of tidal channels is much larger (factor of 2) than the upstream river depth for sandy channels. Deposition occurs for channel depths larger than the equilibrium depth.
7. The further deepening (10 to 20%) of an already deep tidal channel (> 15 m; Rotterdam Waterway) has a marginal effect on the tide-integrated transport rates, the deposition rates, and the dredging volumes (no tipping point effects).
8. The change from import to export of sediment at the mouth of a tidal channel (Rotterdam Waterway) occurs for freshwater (river) discharges larger than 1 to 3 m^2/s in the case of a sandy bed.

Acknowledgements Pieter Koen Tonnon and Bas van Maren of Deltares (The Netherlands) are gratefully acknowledged for providing 3D model results for various cases/sites. Both reviewers are acknowledged for their detailed, critical comments to improve the quality of the paper. The studies on the Rotterdam Waterway were done by both co-authors when they were employed by Arcadis Consultancy in The Netherlands. Arcadis is gratefully acknowledged for the permission to publish these results.

References

Amin M (1983) On perturbations of harmonic constants in the Thames estuary. Geophys J R Astron Soc 73(3):587–603

Arcadis 2015 Deepening of Rotterdam Waterway and Botlek; morphology study. Report C03041.002053.0100 (in Dutch)

BAW, Bundes Anstalt für Wasserbau (2006) Gutachten zur ausbaubedingten Aenderung der morphodynamischen Prozesse (in German), Report H1c, www.fahrrinnenausbau.de

Brenou I, Le Hir P (1999) Modelling the turbidity maximum in the Seine estuary (France). Estuar Coast Shelf Sci 49:525–544

Burchard H, Baumert H (1998) The formation of estuarine turbidity maxima due to density effects in the salt wedge. A hydrodynamic process study. J Phys Oceanogr 28(2):309–320

Chatwin PC (1976) Some remarks on the maintenance of the salinity distribution in estuaries. Estuar Coast Mar Sci 4:555–566

Chernetsky A, Schuttelaars H, Talke S (2010) The effect of tidal asymmetry and temporal settling lag on sediment trapping in tidal estuaries. Ocean Dyn 60:1219–1241

De Jonge VN, Schuttelaars HM, Van Beusekom JEE, Talke SA, De Swart HE (2014) The influence of channel deepening on estuarine turbidity levels and dynamics, as exemplified by the Ems estuary. Estuar Coast Shelf Sci 139:46–59. https://doi.org/10.1016/j.ecss.2013.12.030

Deltares (2011) Tidal phenomena in the Scheldt estuary, part 2. Report 1204410, Delft

Deltares/Delft Hydraulics (1980) Computation of siltation in dredged trenches. Report R1267 V, Delft

DiLorenzo JL, Huang P, Thatcher ML, Najarian TO (1993) Dredging impacts on Delaware Estuary tides. Presented at the 3rd International Conference on Estuarine and Coastal Modeling III. Oak Brook, Illinois, pp 86–104

Dronkers JJ (1964) Tidal computations in rivers and coastal waters. North-Holland, New York, p 518

Familkhalili R, Talke SA (2016) The effect of channel deepening on tides and storm surge: a case study of Wilmington, NC. Geophys Res Lett 43:9138–9147

Friedrichs CT (2010) Barotropic tides in channelized estuaries. Contemporary issues in estuarine physics. Cambridge University Press, pp 27–61

Friedrichs CT, Aubrey DG (1988) Non-linear tidal distortion in shallow well-mixed estuaries; a synthesis. Estuar Coast Shelf Sci 27:521–545

Hansen DV, Rattray M (1965) Gravitational circulation in straits and estuaries. J Mar Res 23:104–122

Herrling G, Niemeyer HD (2008) Comparison of the hydrodynamic regime of 1937 and 2005 in the ems estuary by applying mathematical modeling. Harbasins report, 30 p

Herrling G, Elsebach J, Ritzmann (2014) Evaluation of changes in the tidal regime of the ems-Dollard and lower Weser estuaries by mathematical modelling. Die Kuste 81:353–368

Hollebrandse FAP (2005) Temporal development of the tidal range in the southern North Sea. MSc. Thesis, Civil Engineering, Delft University of Technology, Delft

Kuijper K, Van Rijn LC (2011) Analytical and numerical analysis of tides and salinities in estuaries; Part II: salinity distributions in prismatic and convergent tidal channels. Ocean Dyn 61:1743–1765

Lesser G, Roelvink JA, Van Kester JATM, Stelling GS (2004) Development and validation of a three-dimensional morphological model. J Coast Eng 51:883–915

Lorentz HA (1922) Including resistance in tidal flow equations (in Dutch). De Ingenieur, p. 695, The Netherlands

Lorentz HA (1926 Report Commission Zuiderzee 1918–1926 (in Dutch). Den Haag

Nikuradse J (1933) Strömungsgesetze in rauhen Rohren. Forschungsarbeiten aus dem Gebiete des Ingenieurwesens, Ver. Deut. Ing. Forschungsheft 361, Berlin, Germany

Prandle D (1985) On salinity regimes and the vertical structure of residual flows in narrow estuaries. Estuar Coast Shelf Sci 20:615–635

Prandle D (2004) Saline intrusion in partially mixed estuaries. Estuar Coast Shelf Sci 59:385–397

Prandle D (2009) Estuaries: dynamics, mixing, sedimentation and morphology. Cambridge University Press

Rijkswaterstaat (2017) Internet tidal database (getij.rws.nl)

Talke SA, De Swart HE, Schuttelaars HM (2009) Feedback between residual circulations and sediment distribution in highly turbid estuaries: an analytical model. Cont Shelf Res 29:119–135. https://doi.org/10.1016/j.csr.2007.09.002

Van de Kreeke J, Haring J (1979) Equilibrium flow areas in Rhine-Meuse Delta. Coast Eng 3:97–111

Van Maren DS, Van Kessel T, Cronin K, Sittoni L (2015a) The impact of channel deepening on estuarine sediment concentration. Cont Shelf Res 95:1–14

Van Maren DS, Winterwerp JC, Vroom J (2015b) Fine sediment transport into the hyper-turbid lower Ems River: the role of channel deepening and sediment-induced drag reduction. Ocean Dyn 65:589–605. https://doi.org/10.1007/s/10236-015-0821-2

Van Rijn LC (1984a) Sediment transport, part I: bed load transport. J Hydraul Eng ASCE 110(10)

Van Rijn LC (1984b) Sediment transport, part II: suspended load transport. J Hydraul Eng ASCE 110(11):1613–1641

Van Rijn LC (1984c) Sediment transport, part III: bed forms and alluvial roughness. J Hydraul Eng ASCE 110(12)

Van Rijn LC (1987) Mathematical modelling of morphological processes in the case of suspended sediment transport. Doctoral Thesis. Department of Civil Engineering, Delft University of Technology, Delft, The Netherlands

Van Rijn LC (1993) Principles of sediment transport in rivers, estuaries and coastal seas. www.aquapublications.nl

Van Rijn LC (2007) Unified view of sediment transport by currents and waves, I, II, III. ASCE J Hydraul Eng 133(6):649–667 668–689, No. 7, 761–775

Van Rijn LC (2011a) Principles of fluid flow and surface waves in rivers, estuaries and coastal seas. www.aquapublications.nl

Van Rijn LC (2011b) Analytical and numerical analysis of tides and salinities in estuaries; Part I: tidal wave propagation in convergent tidal channels. Ocean Dyn 61:1719–1741

Van Rijn LC (2015) Principles of sedimentation and erosion engineering in rivers, estuaries and coastal seas. www.aquapublications.nl

Voogt L, Van Rijn LC, Van Den Berg JH (1991) Sediment transport of fine sands at high velocities. J Hydraul Eng ASCE 117:7

Winterwerp JC (2001) Stratification effects by cohesive and non cohesive sediment. J Geophys Res 106(C10):22,559–22,574

Winterwerp JC (2011) Fine sediment transport by tidal asymmetry in the high-concentrated Ems river: indications for a regime shift in response to channel deepening. Ocean Dyn 61:203–215

Winterwerp JC, Wang ZB (2013) Man-induced regime shifts in small estuaries—I: theory. Ocean Dyn. https://doi.org/10.1007/s10236-013-0662-9